Ide and Nomura
Progress in Earth and Planetary Science (2022) 9:67
https://doi.org/10.1186/s40645-022-00523-1

Progress in Earth and Planetary Science

RESEARCH ARTICLE

Open Access

Forecasting tectonic tremor activity using a renewal process model

Satoshi Ide[1*] and Shunichi Nomura[2]

Abstract

In many tectonically active regions of the world, a variety of slow deformation phenomena have been discovered and collectively termed slow earthquakes. Tectonic tremor is the high-frequency component of slow earthquakes and can be analyzed to monitor the overall slow deformation process, both spatially and temporally. Although tectonic tremor activity is complex, it does possess some characteristic patterns, such as spatial segmentation, a quasi-periodic recurrence, migration, and tidal modulation. These features are helpful for forecasting future activity if they are properly modeled in a quantitative manner. Here, we propose a stochastic renewal process to standardize and forecast tectonic tremor activity in the Nankai subduction zone, southwest Japan, using a 12.5-year tremor catalog that is divided into a 10-year estimation period and 2.5-year forecasting period. We group the tremor events into small rectangular 10-km regions and observe that the distribution of inter-event times is nearly bimodal, with the short and long inter-event times representing the characteristic times of nearby tremor interactions and long-term stress accumulation processes, respectively. Therefore, as the probabilistic distribution for the renewal process, we adopt a mixture distribution of log-normal and Brownian passage time distributions for the short and long inter-event times, respectively. The model parameters are successfully estimated for 72% of the entire tremor zone using a maximum likelihood method. This standard model can be used to extract anomalous tremor activity, such as that associated with long-term slow-slip events. We derive a scaling relationship between two characteristic times, the relative plate motion, episodicity of tremor activity, and tremor duration by characterizing the spatial differences in tremor activity. We confirm that the model can forecast the occurrence of the next tremor event at a given reference time for a certain prediction interval. This study can serve as a first step for implementing more complex models to improve the space–time forecasting of slow earthquakes.

Keywords: Slow earthquake, Tectonic tremor, Renewal process, Inter-event time, Probabilistic forecast, Nankai subduction zone, Scaling relationship

1 Introduction

Tectonic tremors are weak intermittent ground-shaking events whose energy is predominantly in the 1–10-Hz frequency range. Since their discovery in the Nankai subduction zone by Obara (2002), they have been found in various subduction zones and other tectonically active regions around the world (Beroza and Ide 2011; Obara and Kato 2016). They are closely related to geodetically detected slow-slip events (SSEs) and very-low-frequency earthquakes (VLFEs), which occur almost simultaneously at similar locations and are defined by seismic signals in the frequency range of 0.01–0.10 Hz. While all these phenomena may be considered a single slow earthquake process (Ide et al. 2007), tectonic tremors and VLFEs are both known to emit continuous signals (Ide 2019; Masuda et al. 2020); it might be therefore appropriate to consider tectonic tremors as the high-frequency component of broadband slow earthquakes in the seismological frequency band. We also consider the otherwise known

*Correspondence: ide@eps.s.u-tokyo.ac.jp

[1] Department of Earth and Planetary Science, The University of Tokyo, 7-3-1 Hongo, Bunkyo, Tokyo 113-0033, Japan
Full list of author information is available at the end of the article

Springer Open

© The Author(s) 2022. **Open Access** This article is licensed under a Creative Commons Attribution 4.0 International License, which permits use, sharing, adaptation, distribution and reproduction in any medium or format, as long as you give appropriate credit to the original author(s) and the source, provide a link to the Creative Commons licence, and indicate if changes were made. The images or other third party material in this article are included in the article's Creative Commons licence, unless indicated otherwise in a credit line to the material. If material is not included in the article's Creative Commons licence and your intended use is not permitted by statutory regulation or exceeds the permitted use, you will need to obtain permission directly from the copyright holder. To view a copy of this licence, visit http://creativecommons.org/licenses/by/4.0/.

phenomenon of low-frequency earthquakes (LFEs) as either a particularly isolated form or building block of tectonic tremors (Shelly et al. 2007a). Tremors are considered a proxy for SSEs due to the high degree of overlap between their source regions (Bartlow et al. 2011; Hirose and Obara 2010). However, it should be noted that tremors are not representative of every type of slow deformation since tremors are not strictly collocated with long-term SSEs (Kostoglodov et al. 2010; Yoshioka et al. 2015) and SSEs may occur without tremors (Kobayashi 2017; Miyazaki et al. 2006).

The Nankai subduction zone has a history of repeated large earthquakes (e.g., Ando 1975), with the next large earthquake expected in the near future (e.g., Hashimoto 2022). It is reasonable to assume that the slow earthquakes in the Nankai region are closely related to the preparation process for a huge earthquake, as some observational (Ito et al. 2013; Shelly 2010) and modeling studies (Matsuzawa et al. 2010) have suggested that there are changes in slow earthquake activity before a major earthquake. However, to detect such changes immediately before a huge earthquake, it is essential to characterize the normal seismic activity in an objective and quantitative way. Furthermore, the objective and quantitative recognition of normal seismic activity can be used to forecast future activity. Understanding the nature of tectonic tremors, evaluating past tremor activity, and forecasting future tremor activity are necessary steps to elucidate slow deformation processes at plate boundaries.

Previous studies have revealed various features of tectonic tremors. Tectonic tremors are not uniformly distributed over plate boundaries, but rather segmented tremor activity at various scales (Brudzinski and Allen 2007; Ide 2010; Obara 2010). These segmented seismogenic structures are apparently controlled by the geometry of the plate boundary and the direction of plate subduction. Coherent and episodic tremor activity occurs in these segments, and often migrates slowly at ~ 0.1 m/s in the along-strike direction, which is along the trench axis of the subduction zone (Dragert et al. 2004; Ito et al. 2007). During this slow migration of tremors, faster migration occurs in various modes (Ando et al. 2012; Ghosh et al. 2010; Houston et al. 2011; Ide 2010, 2012; Shelly et al. 2007b). Episodic tremor activity is often repeated at around some time constant that is characteristic for a given region and sometimes exhibits a depth dependence (Wech and Creager 2011). This time constant has been quantified for various tremor regions and has been reported to be correlated with the average tremor duration (Idehara et al. 2014).

A striking feature of tectonic tremors is their strong sensitivity to tidal stresses (Nakata et al. 2008; Rubinstein et al. 2008; Shelly et al. 2007b; Thomas et al. 2012). This tidal sensitivity is also related to the recurrence period (Thomas et al. 2012) and duration (Ide 2010), such that tremors with short recurrence periods and short durations are generally more sensitive to tidal stresses. This is well explained by mechanical models, where the tremors occur in isolated patchy regions that are loaded by a surrounding region of stable sliding (Ando et al. 2010; Nakata et al. 2011). The tidal sensitivity is not uniform at a regional scale because the tremor duration and amplitude vary greatly at shorter (kilometer) scales and are controlled by the spatial structure of the tremors. Wang et al. (2018) used a hidden Markov model to identify the characteristic spatial structure of the tremors in southwest Japan as small clusters that are connected by larger "subsystems." Aiken and Obara (2021) also grouped tremors into clusters based on their spatiotemporal proximity and discussed scaling laws based on the characteristics of each cluster.

Few studies have attempted to forecast tremor activity, even though the above-mentioned features of tectonic tremors may be utilized for forecasting future tectonic tremor activity. Wang et al. (2018) forecasted tremor activity in a relatively short time window of only two days via a Markov process, where the probability of future events does not depend on the long-term tremor history. Conversely, the forecasting of ordinary earthquakes based on past seismicity is a popular approach, as indicated by many of the probabilistic models tested in the Collaboratory for the Study of Earthquake Predictability project (Jordan 2006). In particular, the Epidemic Type Aftershock Sequence (ETAS) model (Ogata 1988), which is a point process model that assumes a background seismicity rate and a triggering process, is the most effective approach for the probabilistic forecasting of future seismicity and detection of anomalous activity, such as earthquake swarms. However, the ETAS model cannot explain the quasi-periodic occurrence of earthquakes since it does not incorporate long-term stress accumulation processes. A popular model for the long-term forecasting of large repeating earthquakes is the Brownian passage time (BPT) model, which approximates the stress accumulation via a Brownian process and regards any repeating seismicity as a renewal process (Matthews et al. 2002).

Here, we develop a probabilistic model for tremor activity as a framework for characterizing the spatiotemporal variations in tremor activity and forecasting future tremor events in the Nankai subduction zone, where tremors are continuously monitored by high-quality seismic observation networks. We consider quasi-periodic tremor activity as a renewal process that is characterized by a BPT-like probability distribution. However, there are several problems with modeling tremor activity using a renewal process. Unlike characteristic repeating earthquakes, tremors

are clearly not independent events, but rather occur as episodic slip sequences on multiple nearby sources. It is also almost impossible to estimate the number of sources in a given fixed region because the minimum unit of the tremor source is difficult to define, unlike in ordinary earthquake analyses. Furthermore, renewal processes are not additive, such that we cannot simply mix them for multiple sources. Therefore, we employ a BPT-like distribution to express the long-term quasi-periodic occurrence of a fuzzy group of tremor sources and adopt another distribution to express any short-term processes within the group. The observed episodic tremor activity is approximated by this mixture distribution, which is defined by several parameters, for each rectangular segment of the tremor zone. We note that this model is oversimplified to explain complex tremor activity. For example, tremors that are triggered by large teleseismic earthquakes (e.g., Miyazawa and Brodsky 2008) cannot be explained in this framework. Nevertheless, we demonstrate that such a simple model is useful for extracting unusual temporal variations, evaluating the spatial characteristics of the tremors, and making a quantitative statistical forecast.

The remainder of this paper is organized as follows. Section 2 provides an overview of the tectonic tremor activity in the Nankai subduction zone and introduces the tremor catalog, from which we use the inter-event times of successive tremor events as data. We propose a mixture model with five parameters to explain the approximately bimodal distribution of the inter-event times. In Sect. 3, we introduce a maximum likelihood estimation method for the parameters, discuss the estimated values and errors, and evaluate the goodness of fit of the model. In Sect. 4, we discuss the parameter values that are obtained for each region and their meanings. We specifically employ a regression analysis among the parameters, which provides a scaling relation for the long-term tremor recurrence interval that is determined by the rate of plate subduction, tremor duration, tremor episode duration, and number of tremors in each episode. This means that the tremors essentially reflect a simple process of accumulation and release in the form of interplate slip movement. In Sect. 5, we calculate the probability of a future tremor occurrence, predict the time interval when the next tremor event will occur after a given reference time, and observe that the model generally performs as expected. We discuss the possibility of incorporating the tidal stress response and spatiotemporal extension in Sect. 6 and provide the conclusions in Sect. 7.

2 Data: tectonic tremors in the Nankai subduction zone

2.1 Tectonic tremors in Nankai

Tectonic tremors occur in a band-like region in the Nankai subduction zone, southwest Japan, extending about 1000 km from the Tokai region to the Kii and Shikoku regions (Fig. 1). The tremors are discontinuous in Ise Bay, between the Tokai and Kii regions, and in Kii Channel, between the Kii and Shikoku regions. The tremors occur in ~ 20–30-km-wide zones at ~ 30–40 km depth.

Tremors occurred episodically, with a recurrence interval of a few months, at many locations in the Nankai subduction zone, although some locations experienced almost continuous tremor activity (Fig. 1). Tremor activity often exhibits significant migrations, as shown in Fig. 1. These consist of slow (~ 0.1 m/s) migrations in the strike direction (Ito et al. 2007) and fast (~ 10 m/s) migrations in the slip direction (Shelly et al. 2007a, b; Ide 2012), as well as diffusive migrations (Ide 2010) in a small group of tremors. These migrations mean that each location is dependent on other locations, as this activity cannot be fully explained by temporal changes at each location individually. However, this study only considers the temporal changes in a small area as a first step in probabilistic tremor modeling. Therefore, it should be noted that many of the short time intervals that are discussed below do not represent the recurrence interval of events at a given location, but rather the time delay of the tremor triggering sequence during migration processes.

The tremors in the Nankai subduction zone are modulated by tidal stress variations and exhibit a periodicity that corresponds to the tides (Nakata et al. 2008; Shelly et al. 2007b). However, this tidal sensitivity varies spatially and tends to be small in many areas, especially those with long tremor durations (Ide 2010; Ide and Tanaka 2014; Yabe et al. 2015).

2.2 Tectonic tremor catalog used in this study

Many catalogs of tectonic tremor and LFE have been constructed using various methods, and archived in the Slow Earthquake Database (Kano et al. 2018). Here, we use the tremor catalog of Mizuno and Ide (2019). The analyzed

(See figure on next page.)

Fig. 1 Tectonic tremor catalog for the Nankai subduction zone (Mizuno and Ide 2019), which was used in this study. **a** The epicenter locations are shown as circles and color-coded by depth. The tremors that occurred in the Tokai, Kii, and Shikoku regions are separated by Ise Bay and the Kii Channel, respectively. **b** Space–time plot of the Tokai–Kii region, color-coded by location along a N38°W trend. **c** Space–time plot for the Shikoku region, color-coded by location along a N28°W trend

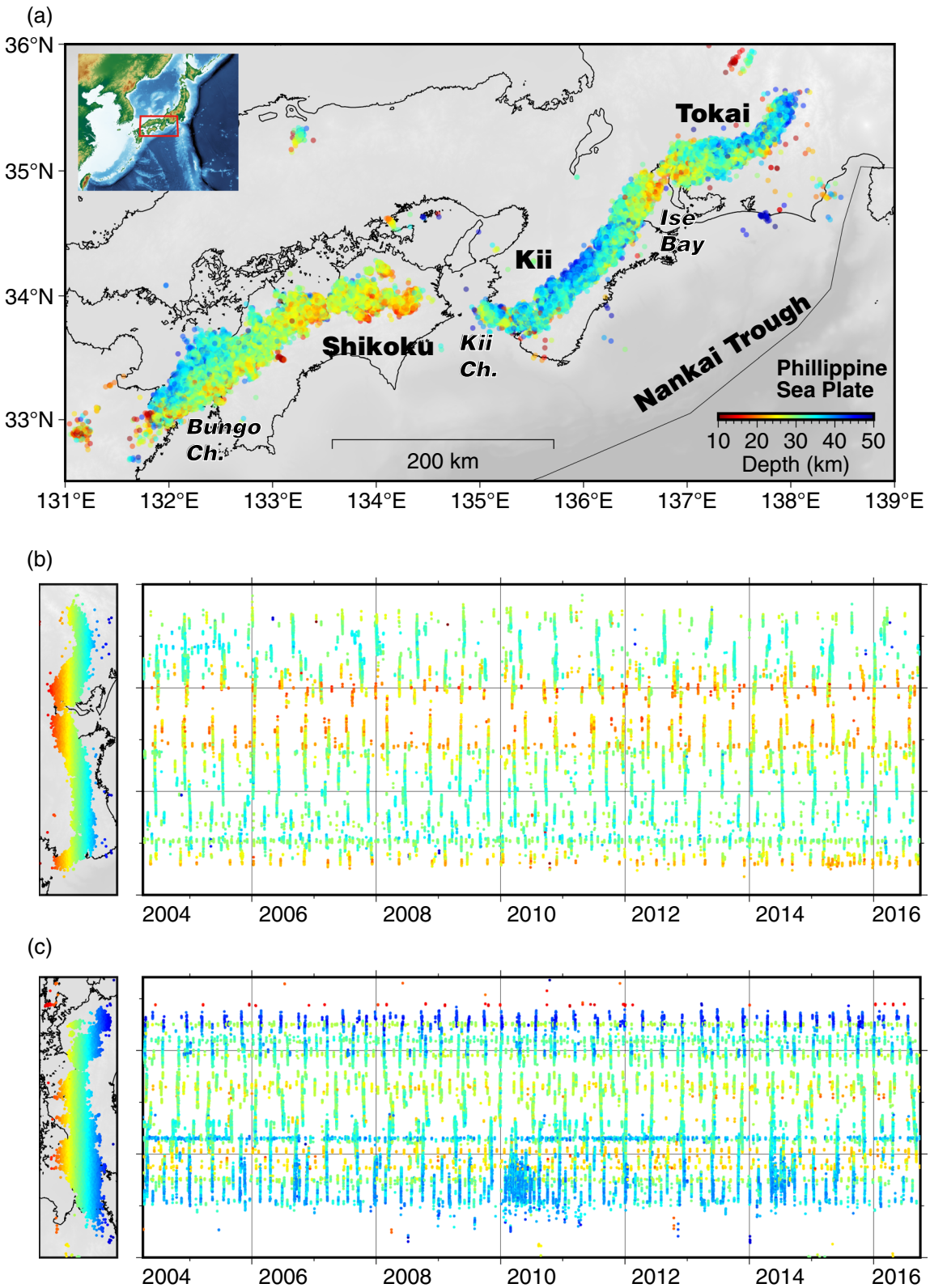

Fig. 1 (See legend on previous page.)

seismic dataset was preprocessed following Ide (2010) and Idehara et al. (2014), and the catalog was constructed using an envelope stacking method similar to that employed by Wech and Creager (2008). Tremors were detected from continuous velocity seismograms of Hi-net, which are managed by the National Research Institute for Earth Science and Disaster Resilience, for the entire Nankai region during the period from April 2004 to September 2016 by employing a sliding 300-s time window with 150-s overlap. The catalog includes multiple events that occurred at different locations within the same time window and were separated by more than ~ 100 km. The duration information for each tremor event was obtained from the full width at half maximum of the amplitude of the stacked envelopes, and the energy magnitude was calculated from the seismic wave energy for the duration of the event.

2.3 Distribution of the inter-event time

We placed grid points at a 0.05° increment across the 33.0–35.6°N, 131.8–138°E region in western Japan, and grouped the tectonic tremors possessing epicenters within ± 0.05° in both latitude and longitude around each grid point. Therefore, each group represents a ~ 10-km rectangular area. The first 10-year period of the catalog (April 2004 to March 2014) was used for the model estimation, and the final 2.5-year period of the catalog was used for the forecasting experiment, which employed the model estimation results. We analyzed the groups that contained more than 300 tremor events during the first 10-year period.

Figure 2 shows example histograms of the inter-event times, which are calculated as the interval between any two consecutive events in each group. The histograms

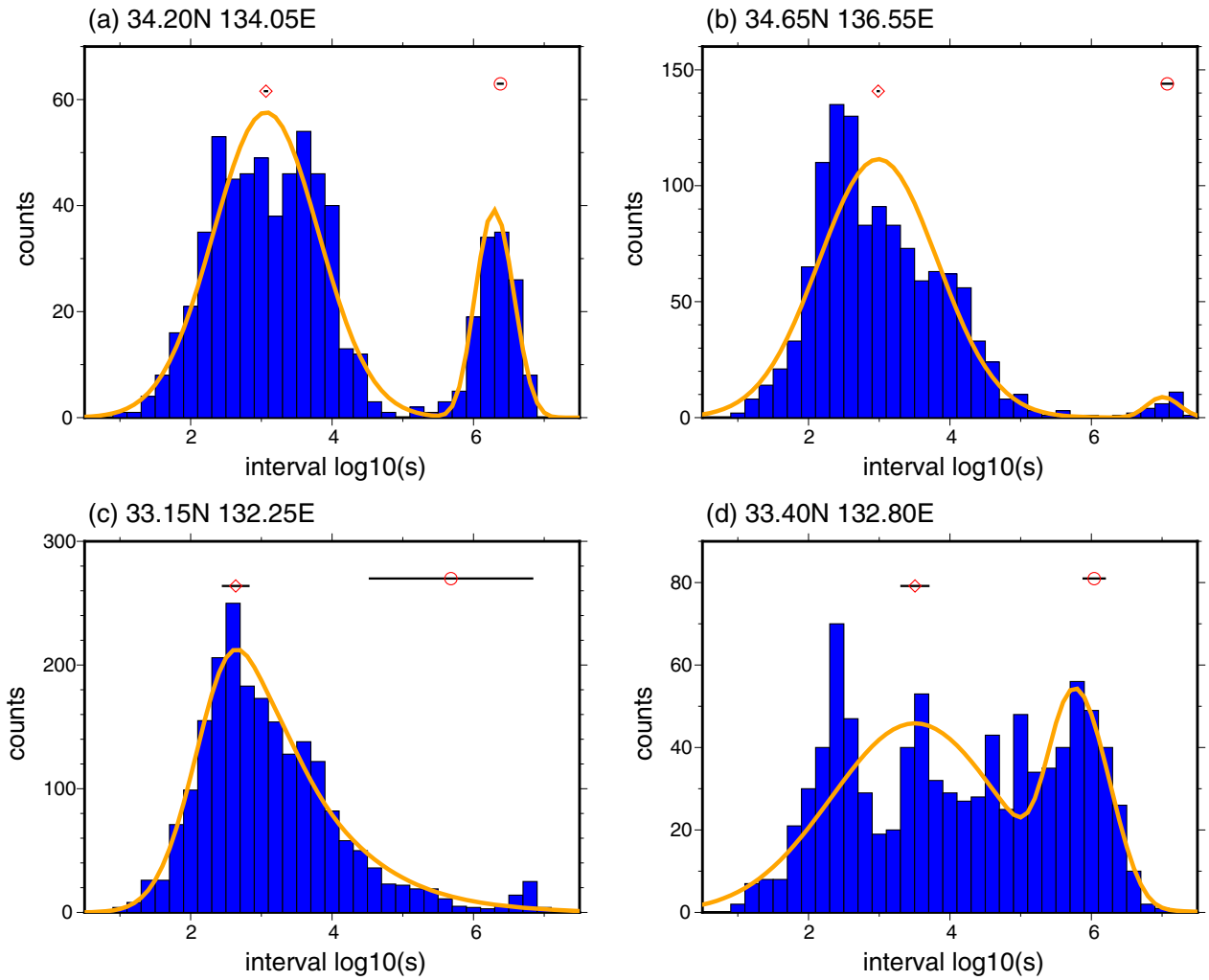

Fig. 2 Histograms of the inter-event times for four groups: **a** 34.20°N, 134.05°E; **b** 34.65°N, 136.55°E; **c** 33.15°N, 132.25°E; and **d** 33.40°N, 132.80°E. The inter-event time counts are shown in blue, and the fitted mixture distribution is plotted as an orange curve. The red circle and diamond at the top of each panel indicate the estimated μ_L and μ_S, respectively, with the error bars showing the standard errors on a logarithmic scale

for most of the groups possess two peaks, which correspond to a long-term loading process and a short-term stress release process with potential migration during episodic activity.

We assume that a tectonic tremor occurs when the stress accumulated by long-term loading reaches a certain value. This assumption is similar to that for characteristic repeating earthquakes. However, loading is not constant and in nature is often subjected to various disturbances. The BPT model, which is based on an inverse Gaussian distribution, approximates this disturbance as a Brownian motion (Matthews et al. 2002). The probability density function of the inter-event time t in the BPT model is expressed as follows:

$$f_{\mathrm{BPT}}(t|\mu_{\mathrm{L}},\alpha)=\sqrt{\frac{\mu_L}{2\pi\alpha^2t^3}}\exp\left\{-\frac{(t-\mu_{\mathrm{L}})^2}{2\mu_{\mathrm{L}}\alpha^2t}\right\}, \quad (1)$$

where μ_{L} is the long-term recurrence period and α represents variations in the period due to the disturbances; these parameters are controlled by the speed and stability of long-term loading processes. This distribution is similar to the more popular log-normal distribution, but it differs when t is large. The BPT model is more convenient for modeling long-term earthquake recurrences using the hazard rate, which we explain later, because the hazard rate of a log-normal distribution will eventually approach zero.

Conversely, the distribution of the short-term inter-event times, which correspond to the stress release process, seems to have a characteristic peak at ~ 1000–10,000 s. This means that tremors are concentrated in a short duration, which is a potential indicator of episodic slow-slip activity (e.g., Frank et al. 2016). There are several possible functional forms to explain this peak. However, it cannot be explained by a very simple stationary Poisson process, as shown in Additional file 1: Fig. S1. Although it may also be approximated by a BPT distribution, we assume a more commonly used log-normal distribution. In fact, the aforementioned characteristics of the log-normal distribution, where the corresponding hazard rate approaches zero for large t, are convenient because the short-term process does not affect the long-term process significantly. Therefore, the probability distribution function for the short peak is written as follows:

$$f_{\mathrm{LN}}(t|\mu_{\mathrm{S}},\sigma)=\frac{1}{\sqrt{2\pi}\sigma t}\exp\left\{-\frac{(\ln t-\ln\mu_{\mathrm{S}})^2}{2\sigma^2}\right\}, \quad (2)$$

where $\ln\ \mu_{\mathrm{S}}$ and σ^2 are the mean and variance of $\ln\ t$, respectively; these parameters reflect the efficiency and heterogeneity of the stress interactions among nearby tremor sources.

The inter-event distribution of our renewal process model is the weighted sum of the above two distributions (Eqs. 1, 2). We define ϕ as the proportion of $f_{\mathrm{LN}}(t)$ to obtain the following relationship:

$$f_{\mathrm{total}}(t|\mu_{\mathrm{L}},\alpha,\mu_{\mathrm{S}},\sigma,\phi)=\phi f_{\mathrm{LN}}(t|\mu_{\mathrm{S}},\sigma)+(1-\phi)f_{\mathrm{BPT}}(t|\mu_{\mathrm{L}},\alpha). \quad (3)$$

This is the mixture distribution with five parameters, $\mu_{\mathrm{L}},\alpha,\mu_{\mathrm{S}},\sigma,$ and ϕ, which are estimated by the real data.

3 Model: estimation and validation of the renewal model

3.1 Maximum likelihood estimation of the model parameters

For a sequence of $n+1$ tremor events that occurred at time $t_0,\ldots,t_n$, n inter-event times $\Delta t_i=t_i-t_{i-1}(i=1,\ldots,n)$ are assumed to obey the mixture distribution. Therefore, the likelihood of the five parameters, $\mu_{\mathrm{L}},\alpha,\mu_{\mathrm{S}},\sigma,$ and ϕ, is given as either:

$$L(\mu_{\mathrm{L}},\alpha,\mu_{\mathrm{S}},\sigma,\phi)=\prod_{i=1}^{n}\left[\frac{\phi}{\sqrt{2\pi}\sigma\,\Delta t_i}\exp\left\{-\frac{(\ln\Delta t_i-\ln\mu_s)^2}{2\sigma^2}\right\}+(1-\phi)\sqrt{\frac{\mu_{\mathrm{L}}}{2\pi\alpha^2\Delta t_i^3}}\exp\left\{-\frac{(\Delta t_i-\mu_{\mathrm{L}})^2}{2\mu_{\mathrm{L}}\alpha^2\Delta t_i}\right\}\right], \quad (4)$$

or the log-likelihood:

$$\ln\ L(\mu_{\mathrm{L}},\alpha,\mu_{\mathrm{S}},\sigma,\phi)=\sum_{i=1}^{n}\ln\left[\frac{\phi}{\sqrt{2\pi}\sigma\,\Delta t_i}\exp\left\{-\frac{(\ln\Delta t_i-\ln\mu_s)^2}{2\sigma^2}\right\}+(1-\phi)\sqrt{\frac{\mu_L}{2\pi\alpha^2\Delta t_i^3}}\exp\left\{-\frac{(\Delta t_i-\mu_L)^2}{2\mu_L\alpha^2\Delta t_i}\right\}\right]. \quad (5)$$

The maximum likelihood estimate based on this likelihood was obtained via the expectation–maximization (EM) algorithm (Dempster et al. 1977), and the estimation error was evaluated using the bootstrap method (e.g., Efron and Tibshirani 1993). One thousand bootstrap samples were resampled from n inter-event times Δt_i, allowing for overlap, and the covariance of these parameters was calculated.

This estimation method was applied to all groups. Figure 2 shows examples of the results for selected groups, and Additional file 1: Fig. S2 shows the results for all

groups. A list of the estimated parameters is given in Additional file 2: Table S1. Reasonable estimates of μ_L and μ_S were obtained for most of the groups, as shown in Fig. 2a, b. The standard error of $\log_{10}\mu_L$ is ~0.1, and the correlation between parameters is small in many cases (Additional file 1: Fig. S3a, b). However, there are some exceptions. The value of μ_L was estimated to be close to μ_S in the westernmost part of the Shikoku region, where many tremors occur (Fig. 2c). The bootstrapping results (Additional file 1: Fig. S3c) indicate that the solution varies among several local minima and that the variation in μ_L is larger than that in μ_S.

The example in Fig. 2d points to the potential of more than three peaks in the histogram of inter-event times within a given tremor group, with this group possessing four peaks (several minutes, one hour, one day, and ten days). The variation in μ_S is larger than that in μ_L for this group (Additional file 1: Fig. S3d), and the other parameters are also poorly determined. One possible explanation for the observation of multiple peaks is that a given group may contain multiple tremor regions with different characteristic time constants due to coarse spatial grouping, such that multiple tremor regions with different characteristic time constants are included in the same group. Another possibility is that a given group may possess several inherent periodicities. We note that clarifying the validity and significance of multiple inter-event times within a given tremor group may be important for understanding tremor mechanisms; however, we have simply excluded such groups from our discussion because there are not many of these groups in our analysis.

When the distribution of inter-event time is quite different from that for the mixture distribution assumed in this study, the standard error of the parameters is very large. Therefore, the results for such groups, which possess a standard error of >0.2 in either $\ln\mu_L$ or $\ln\mu_S$, were not used in the analysis in Sects. 4 and 5.

3.2 Hazard rate in the renewal process

Here, the tremor sequence is modeled as a renewal process, where the probability density of the inter-event time is represented by $f_{\text{total}}(t)$. Therefore, the hazard rate of tremor occurrence at lapse time t since the last tremor event is given by (e.g., Matthews et al. 2002):

$$h(t) = \frac{f_{\text{total}}(t)}{1 - F(t)}, \tag{6}$$

where

$$F(t) = \int_0^t f_{\text{total}}(t')\mathrm{d}t'. \tag{7}$$

The hazard rate that corresponds to the histogram in Fig. 3a is shown in Fig. 3b, c. Immediately after a tremor occurs, a subsequent tremor is likely to occur. However, the rate decreases after this period, such that a subsequent tremor is unlikely to occur; the hazard rate then increases again due to the loading modeled by BPT. Figure 3d, e shows the variations in the hazard rate in this group over long periods. Figure 3d includes 74 events, although about 15 are visually recognized. The hazard rate decreases as shown in Fig. 3b after each event. When several tremors occur in a short time, all of them occur with high hazard rate as shown in Fig. 3e.

3.3 Validation using the transformed time

This probabilistic model can standardize spatially diverse tremor activity. The validity of the standardization is confirmed by transforming the actual time series of events into a transformed time series (Ogata 1988). The transformed inter-event time $\tau(t)$ is calculated using the event occurrence time interval t and hazard rate $h(t)$ as follows:

$$\tau(t) = \int_0^t h(t')\mathrm{d}t'. \tag{8}$$

Let $T(t_i) = \tau(t_1) + \cdots + \tau(t_i)$ be the transformed time of the ith tremor event. Proper modeling of the tremor sequence allows the transformed time series $T(t_1), \ldots, T(t_n)$ to be regarded as a sample from a stationary Poisson process with an occurrence rate of one, such that the number of tremor events and the transform times are approximately linear. More precisely, the validity of the model is determined using the Kolmogorov–Smirnov (KS) test, which states that if the transformed time series satisfies:

$$\max_{i=1,\ldots,n} |T(t_i) - i| < 1.36\sqrt{n}, \tag{9}$$

then the null hypothesis that the transformed time series is sampled from a Poisson process is not rejected at the 5% significance level, and the series is expected to follow a stationary Poisson process.

Figure 4 compares the number of events and the transformed times at two locations. The results for the example in Figs. 2a and 3a, where the modeling was generally successful, are shown in Fig. 4a. A total of 364 (83%) of the 437 groups in this study can be regarded as Poisson processes based on this criterion, with this renewal process modeling approach generally being successful. The number of available groups is reduced to 316 (72%) after applying the above-mentioned criterion for the standard error of $\ln\mu_L$ and $\ln\mu_S$. On the other hand, a large deviation from the straight line is observed at $i = 300$–600 in

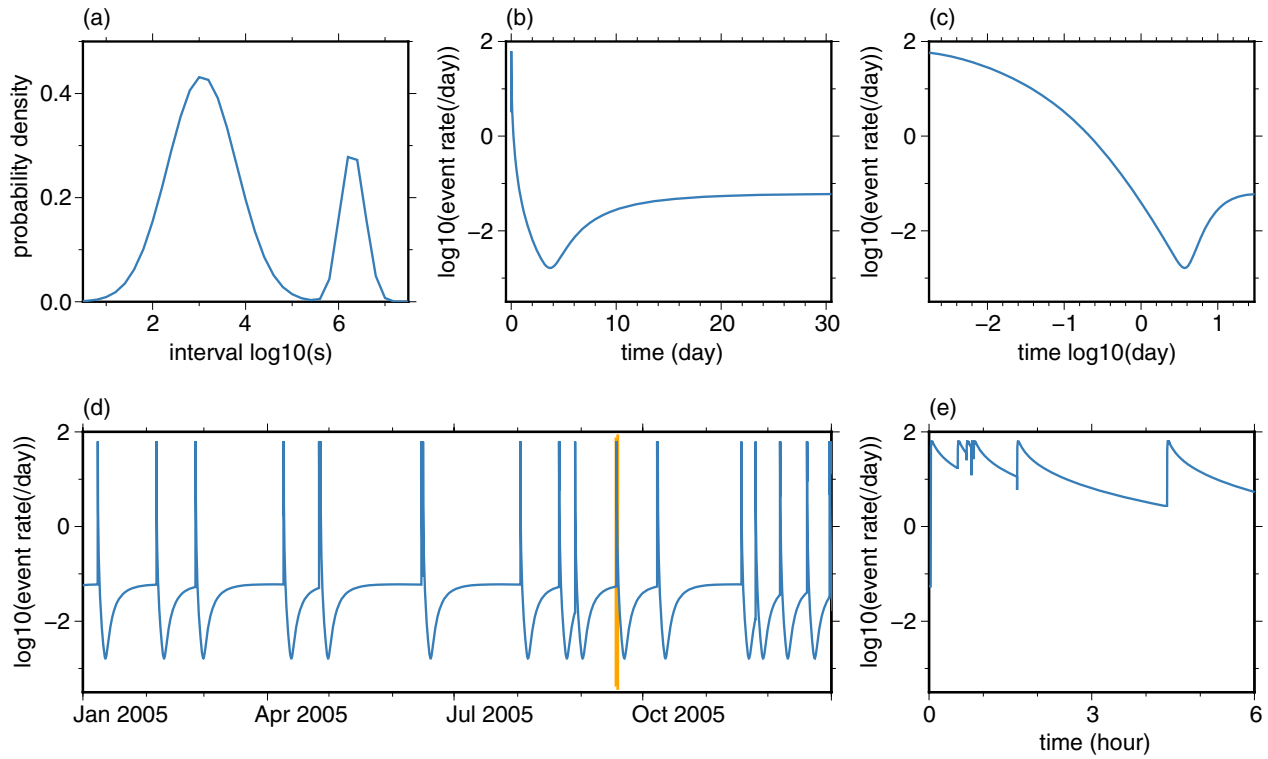

Fig. 3 Converting the probability density function of the inter-event time to the hazard rate. The results for the group centered at 34.20°N, 134.05°E are shown as an example. **a** Probability density function of the inter-event time as a mixture of BPT and log-normal distributions. **b** Hazard rate corresponding to **a**. **c** Log–log plot of **b**. **d** Time series of the hazard rate over one year. **e** Magnified view of the 6-h period indicated by the orange bar in **d**

Fig. 4b, which does not satisfy the condition in Eq. (9). Therefore, this result cannot be regarded as a Poisson process via the KS test. The modeling was likely unsuccessful for these groups because either the tremor behavior changed during the study period, or the groups included unusual periods. The latter is discussed in the following subsection. The distribution of such unsuccessful groups is shown in Additional file 1: Fig. S4. Many of these groups are located near the Tokai and Bungo Channel regions, where long-term SSEs have been reported.

3.4 Quantitative detection of an anomalous period

Ogata (1992) applied the ETAS model to both Japanese and global seismicity and identified a seismically quiescent period before major earthquakes using the deviation of the transformed time series from the Poisson process. Similar deviations have been associated with earthquake swarms and SSEs (Llenos et al. 2009; Okutani and Ide 2011), and volumetric changes around volcanoes (Kumazawa et al. 2016). Positive deviations (i.e., more events than expected) are interpreted to indicate the onset of earthquake swarms and SSEs, whereas negative deviations suggest the influence of stress shadows (e.g., Ogata 2005). It is also possible to detect anomalous periods in the tremor sequences using our renewal process model. We objectively determine an anomalous period from the time series shown in Fig. 4b, which we identified as anomalous in the previous subsection.

The group shown in Fig. 4b is located near the southwestern edge of the study area, where a large SSE and considerable associated tremor activity were observed in 2009–2010 (Fig. 1b) (e.g., Yoshioka et al. 2015). We therefore need to fit a different model because the tremor activity during this period is clearly different from that during the other periods. We consider two cases: Case (1), where the tremor behavior changed at time t_{START}, and Case (2), where the behavior only changed during the period $t_{\mathrm{START}} < t < t_{\mathrm{END}}$. The latter period in Case (1) and the anomalous period in Case (2) are described by another set of model parameters $(\mu'_{\mathrm{L}}, \alpha', \mu'_{\mathrm{S}}, \sigma', \phi')$, such that 10 parameters are estimated via the maximum likelihood method. While the number of parameters to be estimated via the maximum likelihood method is the same in these two cases, Case (2) has an additional change point, at the end of the anomalous period, compared with Case (1). Determining the maximum

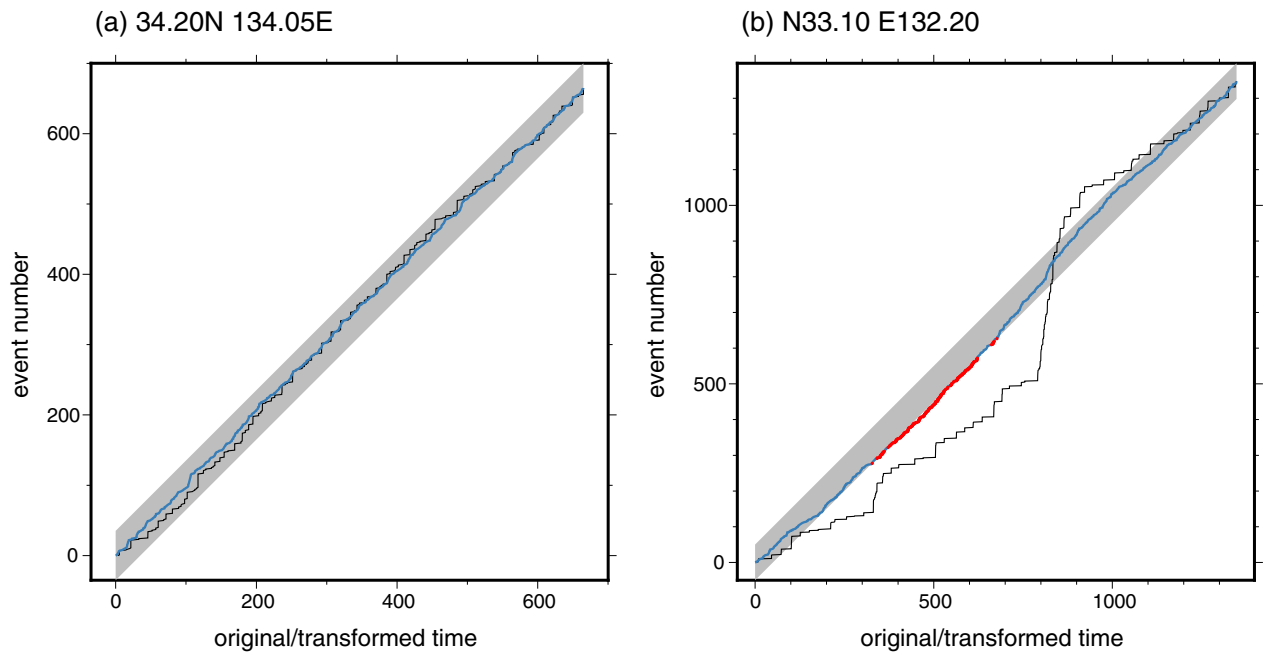

Fig. 4 Kolmogorov–Smirnov test for two groups: **a** 34.20°N, 134.05°E and **b** 33.10°N, 132.20°E. The black line shows the relationship between the event number and the original event time normalized to the event number. The blue line shows the relationship between the transformed time and the event number. The gray zone indicates the region where the null hypothesis is rejected at the 95% level. The blue line outside of this zone is marked by red dots

likelihood solution by varying t_{START} and t_{END} requires these two timings to be treated as change points and given an appropriate penalty (Ogata 1992).

The likelihood was calculated by varying t_{START} in Case (1), and both t_{START} and t_{END} in Case (2), as shown in Fig. 5a, b, respectively. It is natural for the likelihood to increase with the number of parameters. However, the log-likelihood increased by 55.0 in Case (1) and 87.0 in Case (2) with the addition of only five parameters, which is statistically significant based on Akaike's information criterion (AIC). Since the penalties for the change points are calculated to be 9.6 for Case (1) and 32.7 for Case (2) (Ogata 1992; Okutani and Ide 2011), the effective improvements are 45.4 and 54.8, respectively. Therefore, the change-point models are more appropriate than the uniform model, and Case (2) is more appropriate than Case (1) by a small margin.

The maximum likelihood was obtained when the 1348 events in this group were divided into subgroups based on the timings of the 526th event (t_{START} = 08:23:13 on January 29, 2010; all times are given in Japan Standard Time) and 1037th event (t_{END} = 18:56:29 on January 15, 2011). The range over which the log-likelihood is reduced by two roughly corresponds to the 95% confidence interval, which extends from the 424th event (21:39:36 on March 3, 2009) to the 535th event (22:43:59 on January 30, 2010) for t_{START}, and from the 957th event (00:47:07 on August 15, 2010) to the 1052th event (15:14:03 on January 16, 2011) for t_{END}. The beginning of the anomalous period is likely more uncertain because this SSE started with a slow moment release (Yoshioka et al. 2015). The parameters obtained for the maximum likelihood estimates can be used to construct the distribution of inter-event times for each period, as shown in Fig. 5c. The values of μ_{L}' and α' could not be determined precisely due to the short period of available data, whereas the small μ_{S}' value suggests there were many short-term interactions during this period. The transformed time that was calculated using this distribution yields an approximately straight line (Fig. 5d).

This result may seem trivial because the anomaly discussed here was known to be associated with an SSE and was even visually detected in the spatiotemporal tremor distribution. Nevertheless, the objectively determined t_{START} and t_{END} values provide insights into the initiation and termination of the SSE process that was associated with this tremor activity. Such a parameterization can also be used for real-time monitoring to detect anomalous tremor activity.

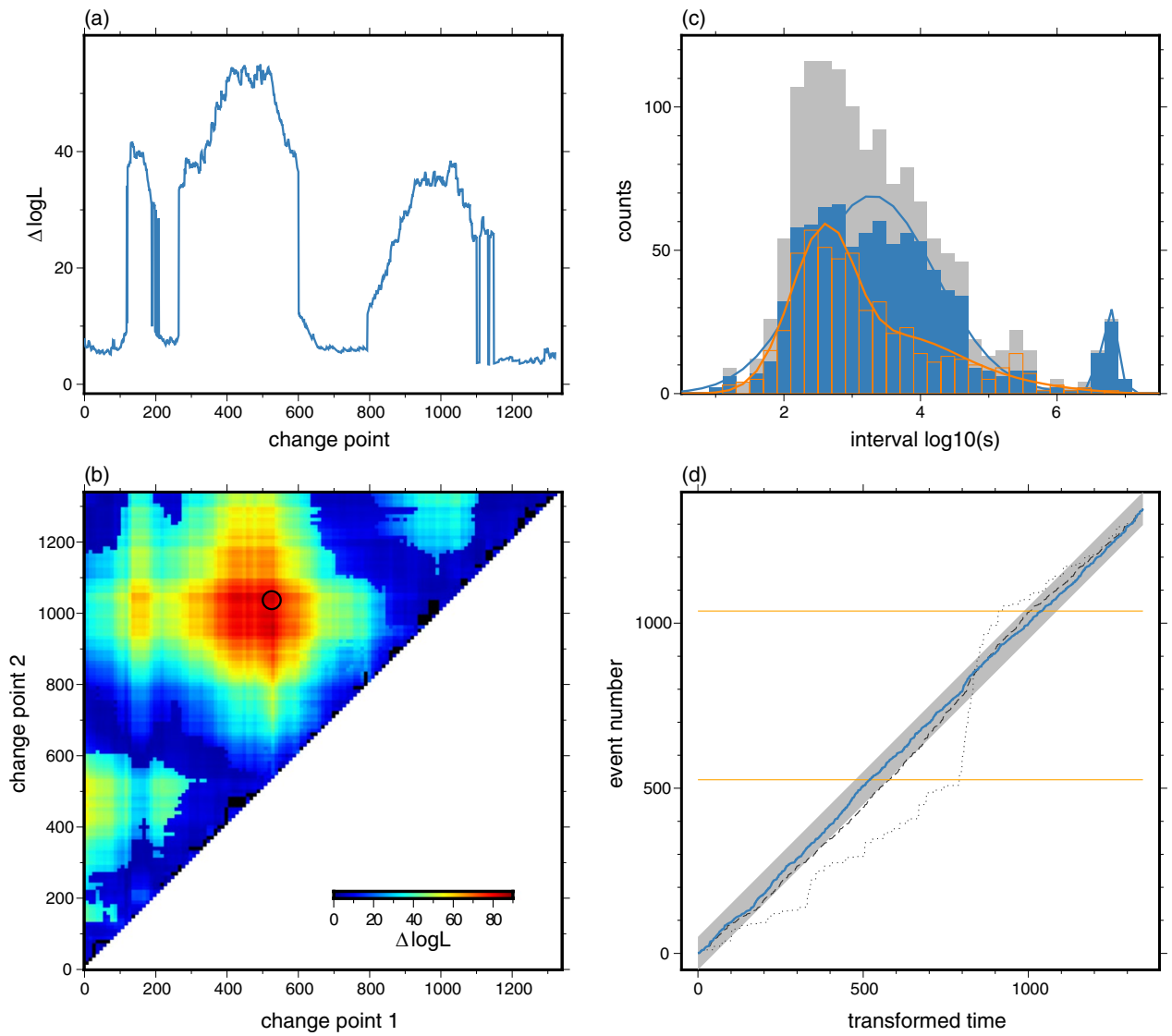

Fig. 5 Anomaly detection for the group at 33.10°N, 132.20°E (Fig. 4b). **a** Difference between the log-likelihood of the model with a single change point and that of the reference model with no change points. **b** Difference between the log-likelihood of the double change-point model and that of the reference model with no change points. The circle shows the location of the best combination of the two change points. **c** Histogram of inter-event times. The gray bars are the original times. The blue and orange bars correspond to the two distributions for the best double change-point model. The fitted distributions are also shown. **d** Comparison of the transformed times and event numbers. The dotted line shows the relationship between the event number and the original event time normalized to the event number. The black dashed and blue lines are the comparisons of the original and double change-point models, respectively. The orange lines show the change points

4 Model estimation results

4.1 Estimated parameters and their spatial distributions

Figure 6 shows the spatial distributions of the five parameters that have been estimated for each tremor group (Additional file 2: Table S1). The maximum likelihood estimates are shown for all of the groups that passed the KS test and possessed standard errors within a factor of 1.22 ($=e^{0.2}$) for the estimated long-term and short-term periods μ_L and μ_S.

The long-term tremor recurrence period μ_L is particularly large in the eastern Tokai region and around Ise Bay and gradually decreases toward the western Kii and Shikoku regions, with a short period of about one month ($10^{6.4}$ s) in some places. This trend is generally similar to that of the time constant estimated by Idehara et al. (2014) and is probably related to large-scale tectonic movement. The subduction rate of the Philippine Sea Plate in the Nankai subduction zone is higher

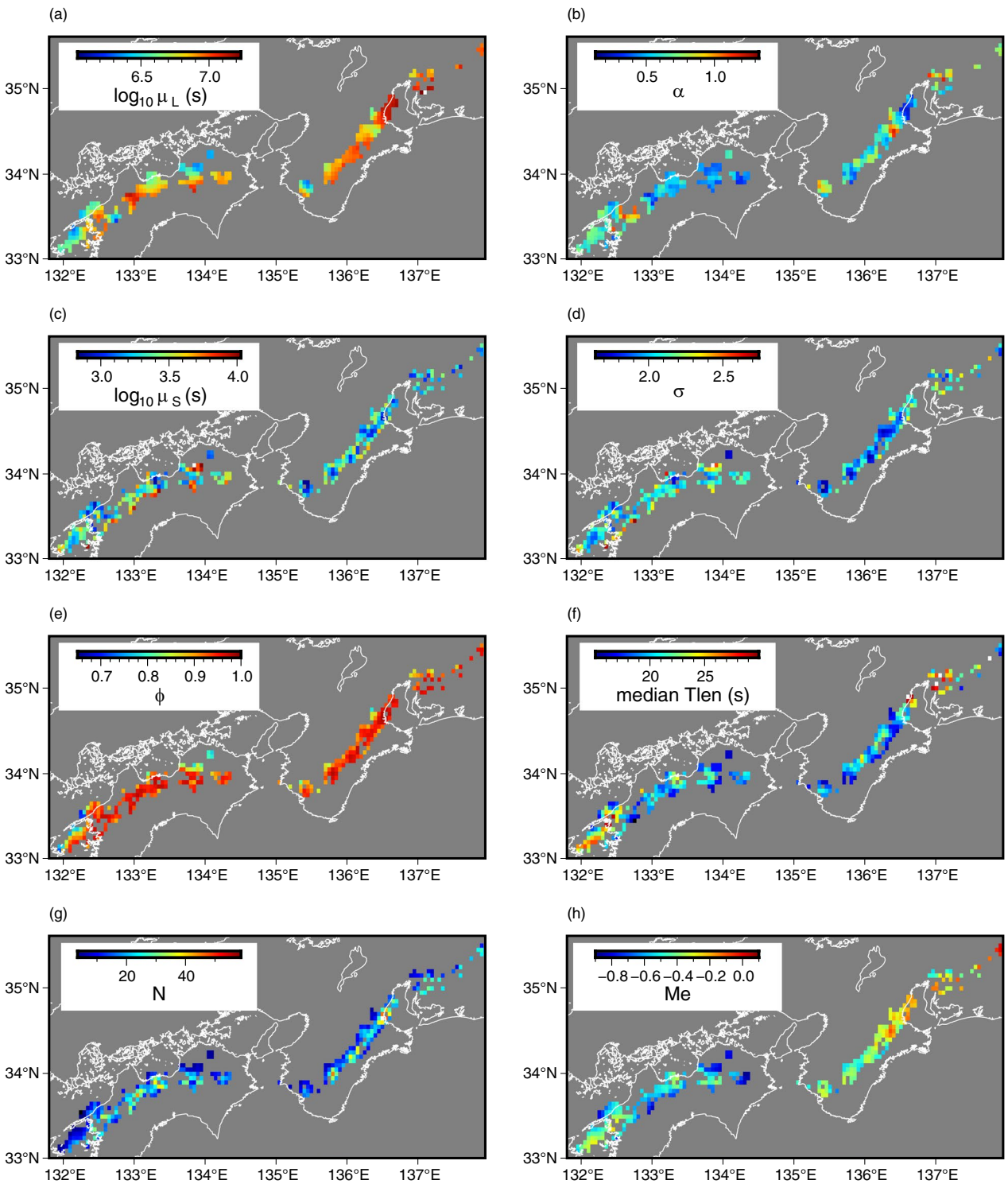

Fig. 6 Spatial distribution of the estimated parameters. **a** Characteristic time of the BPT process, $\log_{10}\ \mu_L$. **b** Coefficient of variation of the recurrence, α. **c** Characteristic time of the log-normal process, $\log_{10}\ \mu_S$. **d** Standard deviation of the log-normal process, σ. **e** Fraction of the log-normal process, ϕ. **f** Median of the tremor duration (Mizuno and Ide 2019)

in the west, and the convergence rate of the plate in the Tokai region is about half of that in the Shikoku region due to the subduction of the Izu Microplate (Heki and Miyazaki 2001; Hori et al. 2004; Miyazaki and Heki 2001). If the amount of interplate slip required to resume tremor activity is uniform everywhere, then a higher convergence rate would yield a smaller μ_L in the western part of Japan. However, secondary factors may be important, especially in the Shikoku region, where μ_L is highly variable at small spatial scales. Annoura et al. (2016) pointed out that the plate convergence rate may control the tremor energy rate. Therefore, both the convergence rate and regional tremor characteristics may control the tremor recurrence period.

The parameter α quantifies the accuracy of the periodicity of the long-term tremor recurrence, and small values were obtained in the eastern Shikoku region and around Ise Bay. These two regions are characterized by quasi-flat subduction; i.e., the dip angle of the plate interface is nearly zero, and the average VLF mechanisms have a nearly horizontal nodal plane (Ide and Yabe 2014). The large α values in the Tokai and Bungo Channel regions may be attributed to the occurrence of long-term SSEs. The parameter σ, which represents the accuracy of the μ_S periodicity, is small in the Kii region. No significant regional variations in μ_S are observed at a large scale. μ_S tends to be smaller in the center of the tremor zone and larger at the periphery; however, this is probably an artifact since the groups near the center of the tremor zone cover a larger portion of episodic tremor activity, whereas those at the periphery do not sample much of this activity due to the constant spatial resolution of 0.05°.

The parameter ϕ represents the fraction of the two mixing distributions, with larger values indicating that most tremors occur as episodic activity and possess short inter-event times. Since ϕ is generally close to one everywhere, we may use another parameter that characterizes the tremor episodicity:

$$N = \frac{1}{1-\phi}, \tag{10}$$

which makes it easier to recognize the difference between the two mixing distributions. N is the number of events that occur during either the long-term tremor recurrence cycle or effectively in an episodic activity. The tremor and LFE episodicity has been quantified in various ways. Some studies have employed an autocorrelation approach to discuss the episodicity (Farge et al. 2021; Frank et al. 2016; Idehara et al. 2014), as such methods capture the degree of clustering and not necessarily the ratio of long-term loading to short-term clustering. Other studies considered "the minimum fraction of days in which 75% of total events occur" (Shelly and Johnson 2011) and "the fraction of the total catalog duration taken up by the largest 2% of the inter-LFE times" (van der Elst et al. 2016) to quantify the short-term clustering within a longer period. For a system with two characteristic time constants, either N or ϕ may give a more general definition of the tremor episodicity than the using criterions with artificial thresholds.

4.2 Scaling relations among the parameters

Figure 7 shows the correlations among the five parameters, with each parameter pair color-coded by tremor duration (T_{len}). There is a weak negative correlation between μ_L and α (Fig. 7a), which indicates that a longer recurrence interval is more periodic and that the groups requiring long-term loading are less affected by the tremor activities of the surrounding groups. Conversely, μ_S and σ exhibit a strong positive correlation (Fig. 7h). One reason for this positive correlation is that the catalog used in this study was constructed using a 150-s window interval, which is a fixed limit of the temporal tremor resolution. Therefore, the variations are small for small μ_S values that are close to the lower limit of 150 s, and vice versa. The mixing ratio ϕ is correlated with all the other parameters (Fig. 7d, g, i, j). A ϕ value close to one indicates a large N value, a small number of cycles in the analysis period, a large long-term recurrence interval μ_L, and a small short-term period μ_S. Then, α and σ also vary with μ_L and μ_S, respectively. Figure 7b shows that μ_S and μ_L tend to be small and large, respectively, for the long-duration (large T_{len}) tremor group, although the direct correlation between μ_L and μ_S is weak. A similar trend is observed for the energy magnitude of tremors. Idehara et al. (2014) also reported that μ_L is correlated with the tremor duration. However, μ_L is not determined using just the duration, as some tremors are short-duration events with large μ_L.

The parameter μ_L is related to various quantities, such as the plate subduction velocity (Fig. 6) and ϕ (or N) (Fig. 7d). The magnitude and/or duration of individual tremors may also be relevant for describing the tremor activity. Furthermore, μ_S is an important parameter for describing any differences in tremor activity, which makes such comparisons valuable in providing additional details on the observed tremor activity. We therefore assessed whether these parameters could be used to explain the variations in μ_L. Specifically, we assumed that μ_L is expressed as a product of the power of μ_S, N, the seismic energy (M_e) and duration (T_{len}) of tremor, and the plate subduction velocity (V_{pl}) and prepared a linear relation for all the groups:

$$\begin{aligned}\log_{10}\mu_L = {} & A\log_{10}\mu_S + B\log_{10}N + CM_e \\ & + D\log_{10}T_{len} + E\log_{10}V_{pl} + F + e.\end{aligned} \tag{11}$$

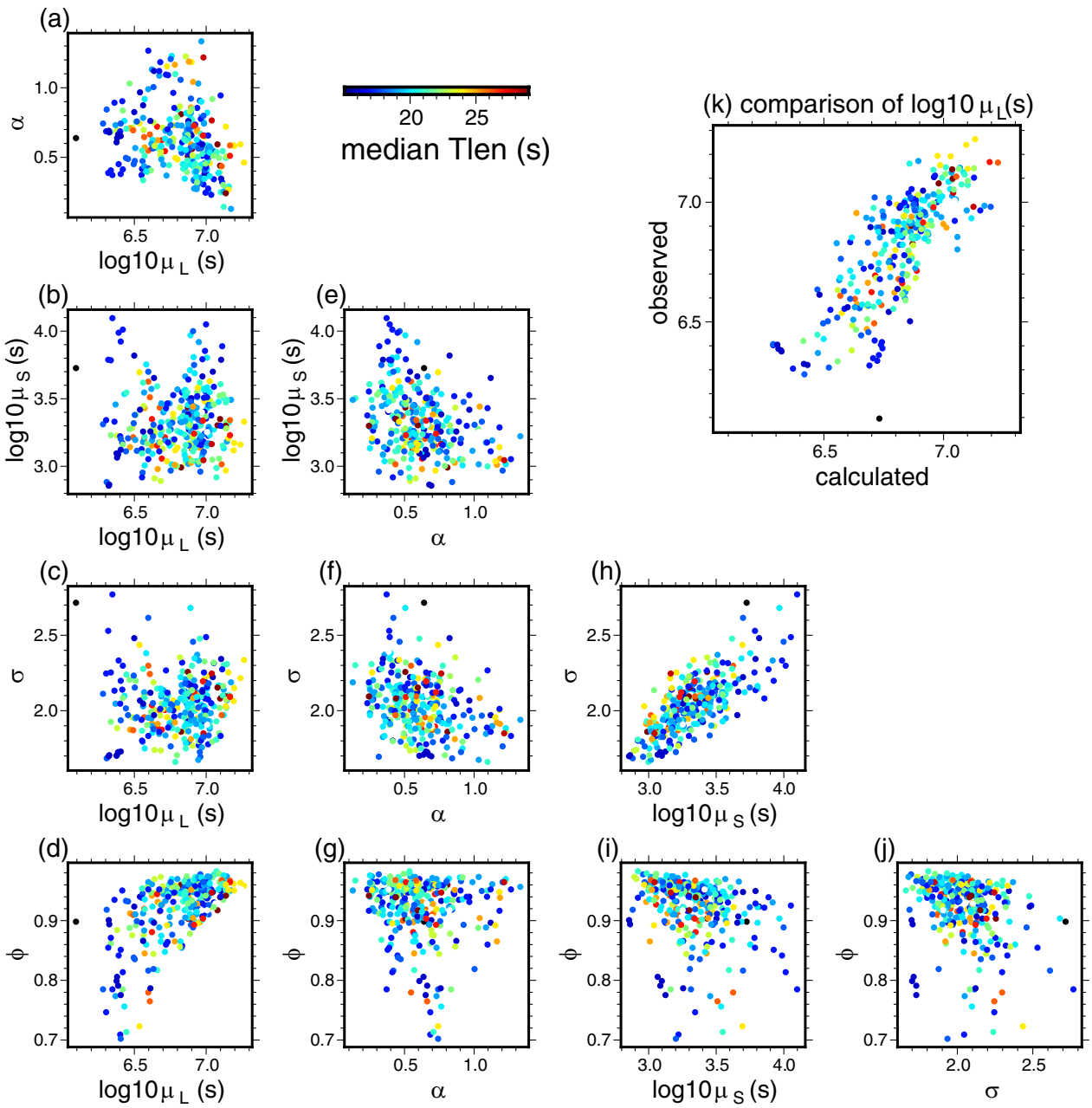

Fig. 7 Relationships between the parameters, estimated from the detected tremors for all the groups. **a** $\log_{10}\ \mu_L$ versus α; **b** $\log_{10}\ \mu_L$ versus $\log_{10}\ \mu_S$; **c** $\log_{10}\ \mu_L$ versus σ; **d** $\log_{10}\ \mu_L$ versus ϕ; **e** α versus $\log_{10}\ \mu_S$; **f** α versus σ; **g** α versus ϕ; **h** $\log_{10}\ \mu_S$ versus σ; **i** $\log_{10}\ \mu_S$ versus ϕ; **j** σ versus ϕ; **k** Comparison of the observed $\log_{10}\ \mu_L$ values and those predicted using Eq. (12). The circles are color-coded by the median tremor duration

We estimated the coefficients A, B, C, D, E, and F using the maximum likelihood method with the assumption that the error e is normally distributed.

We adopted V_{pl} from the plate models that included a rapid decrease in the subduction velocity in the Tokai region (Heki and Miyazaki 2001; Hori et al. 2004). We calculated AIC for all the combinations of coefficients since e naturally decreases as the number of parameters increases; the results are shown in Table 1. Since the AIC with all the coefficients and that without C are almost the same, it is better to ignore the contribution of M_e. All the other coefficients appear to be necessary to explain the variations in μ_L.

Table 1 ΔAIC relative to the minimum value for different sets of coefficients

Coeffs	ΔAIC	Coeffs	ΔAIC	Coeffs	ΔAIC
A, B	113.6	D, E	221.2	B, D, E	88.2
A, C	220.4	A, B, C	64.7	C, D, E	217.6
A, D	269.8	A, B, D	81.2	A, B, C, D	45.1
A, E	224.9	A, B, E	22.5	A, B, C, E	20.3
B, C	140.8	A, C, D	213.1	A, B, D, E	0.0
B, D	136.7	A, C, E	205.6	A, C, D, E	198.9
B, E	94.7	A, D, E	214.3	B, C, D, E	86.0
C, D	236.1	B, C, D	132.1	A, B, C, D, E	0.3
C, E	221.7	B, C, E	94.8		

The intercept F is not shown because it was used in every set of coefficients

The coefficients obtained for the combination of *A*, *B*, *D*, and *E*, together with their standard errors, are as follows:

$$\log_{10}\mu_{\mathrm{L}} \sim (0.39 \pm 0.04)\log_{10}\mu_{\mathrm{S}} + (0.62 \pm 0.03)\log_{10}N + (0.61 \pm 0.12)\log_{10}T_{\mathrm{len}} - (0.57 \pm 0.06)\log_{10}V_{\mathrm{pl}} + (4.43 \pm 0.24). \tag{12}$$

Figure 7k shows a comparison of the data and calculated values of μ_{L}.

We also tested a model that does not include a sudden decrease in V_{pl} in the Tokai region (Miyazaki and Heki 2001) since there are uncertainties in the plate motions and found the combination of *A*, *B*, *D*, and *E* again yielded the optimal μ_{L}, which consisted of the following coefficients:

$$\log_{10}\mu_{\mathrm{L}} \sim (0.41 \pm 0.03)\log_{10}\mu_{\mathrm{S}} + (0.59 \pm 0.03)\log_{10}N + (0.88 \pm 0.11)\log_{10}T_{\mathrm{len}} - (9.89 \pm 0.76)\log_{10}V_{\mathrm{pl}} + (11.64 \pm 0.63). \tag{13}$$

The two regression equations in Eqs. (12) and (13) suggest that μ_{L} depends on V_{pl}^{-1} to the power of 0.57 and 9.89, respectively. Kinematically, $\mu_{\mathrm{L}}V_{\mathrm{pl}}$ represents the amount of accumulated slip deficit for the average recurrence period. Therefore, one would expect μ_{L} to be proportional to V_{pl}^{-1} if episodic tremor activity starts when the slip deficit reaches some constant amount. This hypothesis is not ruled out from the large range of uncertainties in the current plate motion.

The parameter μ_{L} is positively correlated with T_{len}, as noted by Idehara et al. (2014), and with both μ_{S} and *N*. If a fixed small area always slips during a tremor episode and the slip rate is nearly constant, then the amount of slip deficit accumulated during the inter-episode period $\mu_{\mathrm{L}}V_{\mathrm{pl}}$ would be positively correlated with the total time of tremor activity during episodic activity NT_{len}. Furthermore, the fact that μ_{L} is also related to μ_{S} suggests that the background slip, which is thought to be ongoing in the vicinity of tremors during episodic activity (Ando et al. 2010; Nakata et al. 2011), also contributes to the total slip during these tremor episodes. This empirical relation alone cannot determine a specific model for the dynamic slip process of tectonic tremors, but it can place certain constraints on the models.

5 Forecasting model

We conducted a forecasting experiment using the final 2.5 years of the tremor catalog. The mixture distribution with the estimated parameters for the 10-year catalog was used to estimate the timing of the next tremor event for each group. The forecasting methodology follows that in BPT model-based forecasts of characteristic earthquakes (e.g., Matthews et al. 2002).

If the last event occurred at time t_{pre} before a reference time, then the probability density of an event occurring at time t after this reference time is as follows:

$$p(t) = \frac{f_{\mathrm{total}}(t + t_{\mathrm{pre}})}{1 - F(t_{\mathrm{pre}})}. \tag{14}$$

The expected time of the next tremor event is calculated as follows:

$$t_{\mathrm{next}} = \int_0^\infty tp(t)\mathrm{d}t. \tag{15}$$

Let $P(t)$ be the corresponding cumulative distribution function. The ath percentile of the next tremor timing is then obtained by the time $t_{a\%}$ such that $P(t_{a\%}) = a\%$. Using the percentile, we can forecast the timing of the next tremor event by range using prediction intervals such as $t_{2.5\%}$–$t_{97.5\%}$ (95% interval) and $t_{16\%}$–$t_{84\%}$ (68% interval).

The tremor forecasting is conducted as follows. The reference time is first set to 00:00:00 on April 1, 2014, which is the end of the model parameter estimation period. At this time, the optimal conditions should be present for the forecasting, since all the tremor activity information prior to this time is employed in the model. Figure 8a, b shows the cumulative distributions, prediction intervals, expected values, and actual observed times for the two groups in Fig. 2a, b, respectively. In Fig. 8a, the 95% prediction interval spans approximately two months, beginning almost immediately after the reference time, and the 68% interval spans approximately one month. The next tremor actually occurred 40 days later, which falls within the 95% interval but not the 68% interval. In Fig. 8b, the 95% interval extends from 20 days to almost half a year

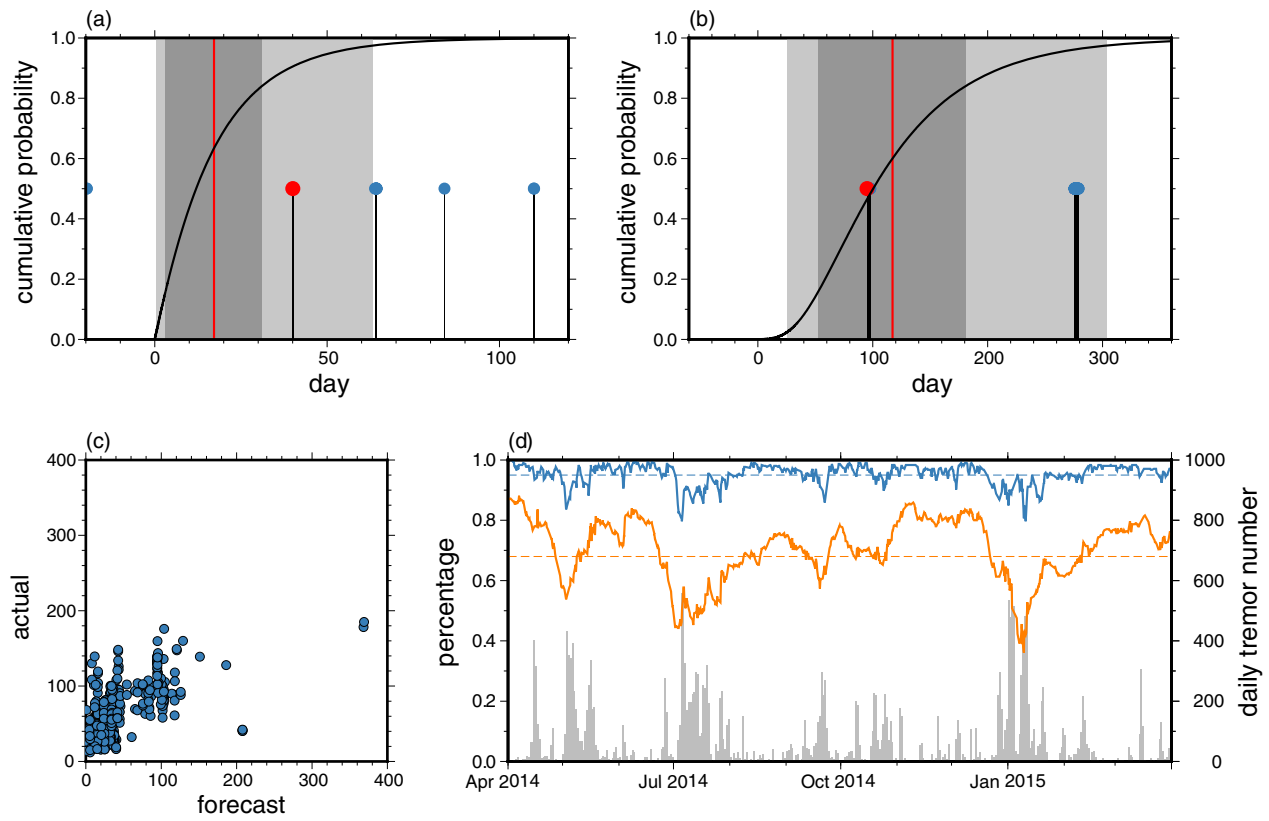

Fig. 8 Example results of the forecasting experiment. The cumulative probabilities (black curves) of the occurrence of the next tremor after the reference time (00:00:00 on April 1, 2014) for the two groups in Fig. 2a, b are shown: **a** 34.20°N, 134.05°E and **b** 34.65°N, 136.55°E. The light-gray and dark-gray bands represent 68% and 95% prediction intervals for the timing of the next tremor events, respectively. The red vertical line shows the expected time of the next tremor event. The circles with vertical bars show the observed timings of the tremor events. The red circle indicates the next tremor event, which is the target of the forecast. **c** Comparison of the forecasted time (mean) of the next tremor events and the actual tremor times. **d** Percentage of the next tremor events that occurred within the 68% (orange) and 95% (blue) prediction interval, calculated for all groups. The dashed horizontal lines show the 68% (orange) and 95% (blue) levels. The gray bars show the daily number of tremor events in the forecasted groups

after the reference time, and the 68% interval spans 80 days, with an expected tremor at 110 days. The next tremor occurred 95 days later.

The same calculation is performed for the 320 groups that yielded estimated parameters with small errors. The resultant predictions better reflect the nature of the BPT model since no tremors occurred at least five days prior to this reference time in any of the groups. The 95% prediction intervals for each group range from a minimum of 40 days to a maximum of 792 days after the reference time; the 68% interval spans approximately half that range, but neither is accurate by more than a few days. Figure 8c shows a comparison of the predicted and actual occurrence times, with 303 (94.7%) and 262 (81.9%) of the 320 groups falling within the 95% and 68% prediction intervals, respectively. The actual occurrence tends to be slightly later than the predicted value at this reference time.

To examine the forecasting performance at different reference times, we repeated the same trial with 1000 randomly selected reference times over a one-year period, beginning at 00:00:00 on April 1, 2014. The proportion of forecasts that fall within the 95% and 68% prediction intervals fluctuates with the time of the year when the forecasts are made (Fig. 8d). The forecasting performance is generally lower when many tremors occur during a given time period. This is probably because the assumed log-normal distribution is too simplistic to accurately represent a short-term recurrence of tremor, which is controlled by various near-field processes, such as tremor migration. However, 95.3% and 70.7% of the events fall within the 95% and 68% intervals of our long-term tremor forecasting results, respectively, which indicates the robust performance of this forecasting model.

The performance gain of the mixture distribution relative to a null model, which is a Poisson process in

this case, is measured based on the likelihood ratio. We calculated the likelihood of the mixture distribution with the estimated parameters from this study and the inter-event times of the forecasting period for each of the 320 groups. The likelihood of a Poisson process is given as:

$$L(\lambda) = \prod_{i=1}^{n} \lambda \exp\{-\lambda \Delta t_i\}, \tag{16}$$

where λ is the event occurrence rate that has been calculated for the estimation period. The mixture distribution always gives a better likelihood, as expected, and the difference in the log-likelihood per inter-event time ranges from 1.5 to 4.8, with a mean of 3.5.

6 Discussion

6.1 Tidal stress effect and the modulated renewal process

Tectonic tremor activity exhibits a strong dependence on the tidal stress across some areas of the Nankai subduction zone (Ide 2010; Nakata et al. 2008; Shelly et al. 2007b). We investigate whether incorporating this dependence will improve the prediction performance using a group that is centered at 34.10°N, 133.90°E, which exhibits a relatively strong dependence on the tidal stress. The tidal stress was calculated at 30 km depth at this location using the code of Yabe et al. (2015) and the PREM velocity model (Dziewonski and Anderson 1981). A focal mechanism with strike 225°, dip 0°, and rake 90° is assumed based on the mechanisms of the VLFEs in the region (Ide and Yabe 2014).

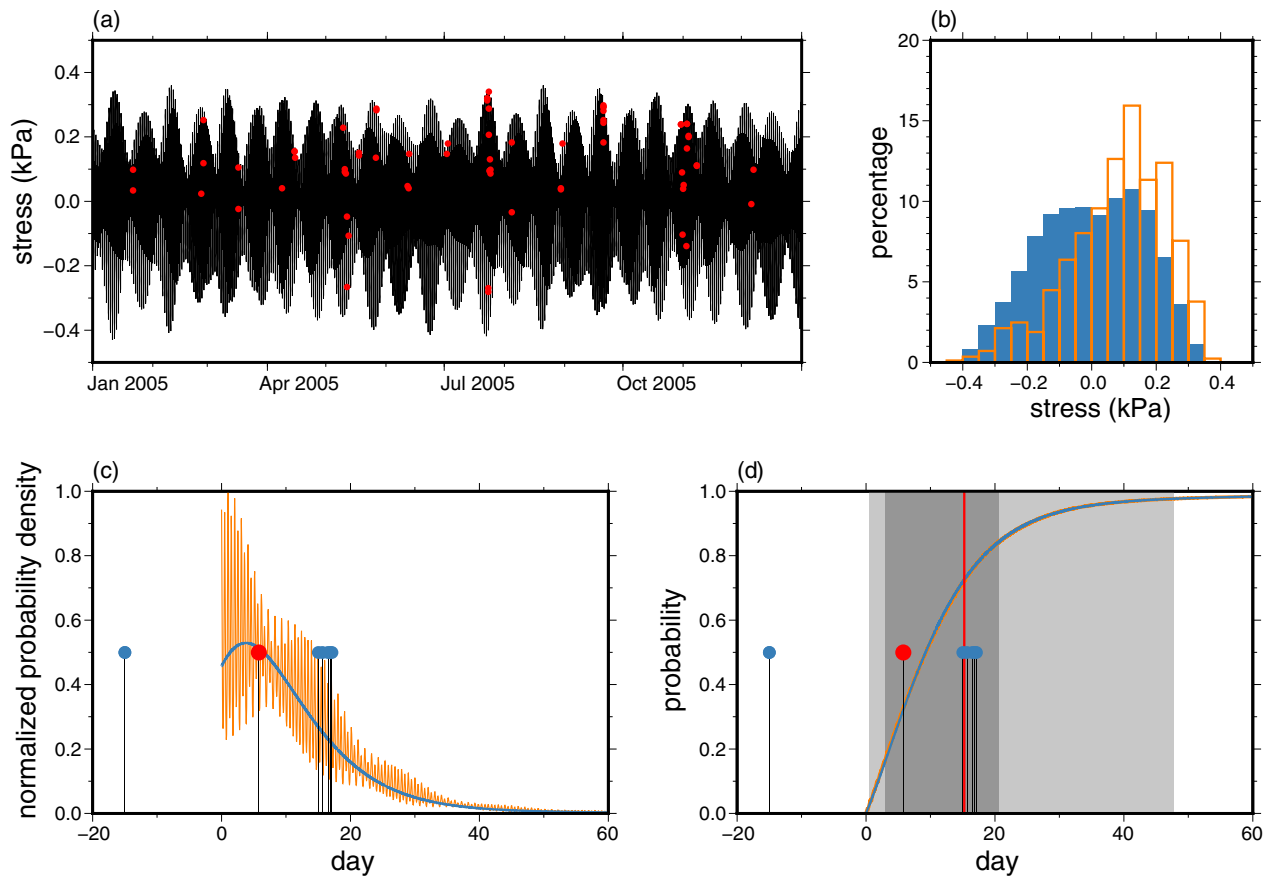

Fig. 9 Evaluation of the tidal stress effect on the tremor group centered at 34.10°N, 133.90°E. **a** Tidal stress level (black line) and timings of tremor events (red dots). **b** Histograms of the tidal stress level at this location for a 10-year period (blue) and timings of the tremor events (orange). **c** Probability density functions of the next tremor events that are estimated using renewal process models with (blue) and without (orange) tidal stress modulation. The circles with vertical bars show the timings of the tremor events. The red circle indicates the next tremor event to be forecasted. **d** Cumulative probability (black curve) of the occurrence of the next tremor after the reference time (00:00:00 on April 1, 2014). The light-gray and dark-gray bands represent the 68% and 95% prediction intervals for the timing of the next tremor events. The red vertical line shows the expected time of the next tremor event. The circles with vertical bars show the observed timing of the tremor events. The red circle indicates the next tremor event, which is the target of the forecast

Tremors occur more frequently when the Coulomb stress is high, as shown in Fig. 9a, and the stress distribution function at the timing of tremor occurrence is clearly shifted in the direction of higher stress compared with the distribution function of stress during the entire period (blue), as shown in Fig. 9b. The ratio between the two, which is the tremor rate at given stress levels, is dependent on an exponential function that has been described in previous studies (Beeler et al. 2013; Thomas et al. 2012; Yabe et al. 2015). This tidal influence is realized in the renewal process model by multiplying the hazard rate $h(t)$, which does not account for tides, by the exponential influence of the tidal stress $\tau(t)$ at time t as follows:

$$h_{\text{tide}}(t;\, \mu_L, \alpha, \mu_S, \sigma, \phi, A_{\text{tide}}) = h\big(t - t_{\text{pre}};\, \mu_L, \alpha, \mu_S, \sigma, \phi\big) \exp\{A_{\text{tide}}\tau(t)\}, \tag{17}$$

where A_{tide} is a parameter that defines the sensitivity to the tidal stress and t_{pre} is the occurrence time of the previous event. This model is known as a modulated renewal process (MRP), and the distribution function for each time can be obtained from the hazard rate in the case of multiplicative modulation (Cox 1972).

For a group consisting of $n+1$ events occurring at time $t_0, \ldots, t_n$, the log-likelihood is expressed using the hazard rate $h_{\text{tide}}(t)$ as follows:

$$\ln L(\mu_{\text{L}}, \alpha, \mu_{\text{S}}, \sigma, \phi, A_{\text{tide}}) = \sum_{i=1}^{n} \ln(h_{\text{tide}}(t_i)) - \int_{t_0}^{t_n} h_{\text{tide}}(t')\mathrm{d}t'. \tag{18}$$

The estimated parameters without considering the tidal effect are:

$$[\log_{10}\mu_{\text{L}}, \alpha, \log_{10}\mu_{\text{S}}, \sigma, \phi] = [6.31, 0.388, 3.78, 2.52, 0.854], \tag{19}$$

with the inclusion of the tidal effect yielding:

$$[\log_{10}\mu_{\text{L}}, \alpha, \log_{10}\mu_{\text{S}}, \sigma, \phi, A_{\text{tide}}] = [6.32, 0.412, 3.92, 2.51, 0.820, 2.18]. \tag{20}$$

Although the individual parameter values are not significantly different between the non-tidal and tidal cases, the log-likelihood for the tidal case increased by about 42.

We expect this renewal process model, which includes the tidal effect, to have a high explanatory power. However, the merit is not clear in the long-term forecast. A forecast of the timing of the next event at the beginning of the forecasting period is shown in Fig. 9c. The rate of occurrence oscillates greatly with the tidal stress changes, which indicates that the tides are a significant contributor to the probability forecast over a very short time frame. However, this tidal contribution is reduced if the time of the next event is evaluated using a cumulative distribution (Fig. 8a, b) and only has a very small effect on the prediction interval (Fig. 9d). The tidal effect would be more important for the forecast at time scales that are much shorter than the tidal periods. However, for short-term forecasting, we must consider other factors, such as tremor migration and interactions.

6.2 The effect of detectability

So far, we used all of the tremor events in the catalog of Mizuno and Ide (2019). The tremor detection limit cannot be homogeneous in time, but rather is controlled by various factors, such as the propagating seismic waves of large earthquakes, tides, weather, and human activity, since tremors radiate signals that are only slightly above the noise level. These changes in the detection limit potentially affect the stochastic modeling results. We are unaware of any previous attempts to estimate the detection limit and completeness of a given tremor catalog, and we note that a thorough evaluation of these effects is beyond the scope of the present study. Nevertheless, we attempt to characterize the sensitivity of our results when only part of a catalog is available by performing the same analysis using one half of the tremor catalog.

The catalog of Mizuno and Ide (2019) provides tremor magnitude information based on the seismic energy. We selected the events with magnitudes larger than the median magnitude for each region that had > 1000 cataloged events. We then estimated the five parameters and their standard errors using the same approach outlined in Sect. 3.1. A comparison of the estimated μ_{L} and μ_{S} values when using the entire catalog and one half of the events is shown in Fig. 10.

These two parameters, which represent the recurrence interval, naturally increase because the number of events is halved for a fixed period. The inter-event time would be exactly doubled when we apply a Poisson process. However, the effect is small in the case of our mixture distribution. The medians of the ratio between the two estimates are 1.28 and 1.57 for μ_{L} and μ_{S}, respectively. This is because these values are determined by characteristic peaks in the inter-event time distribution rather than the overall occurrence rate. μ_{L} is particularly insensitive to the tremor catalog because the long-term recurrence does not change significantly by removing some events

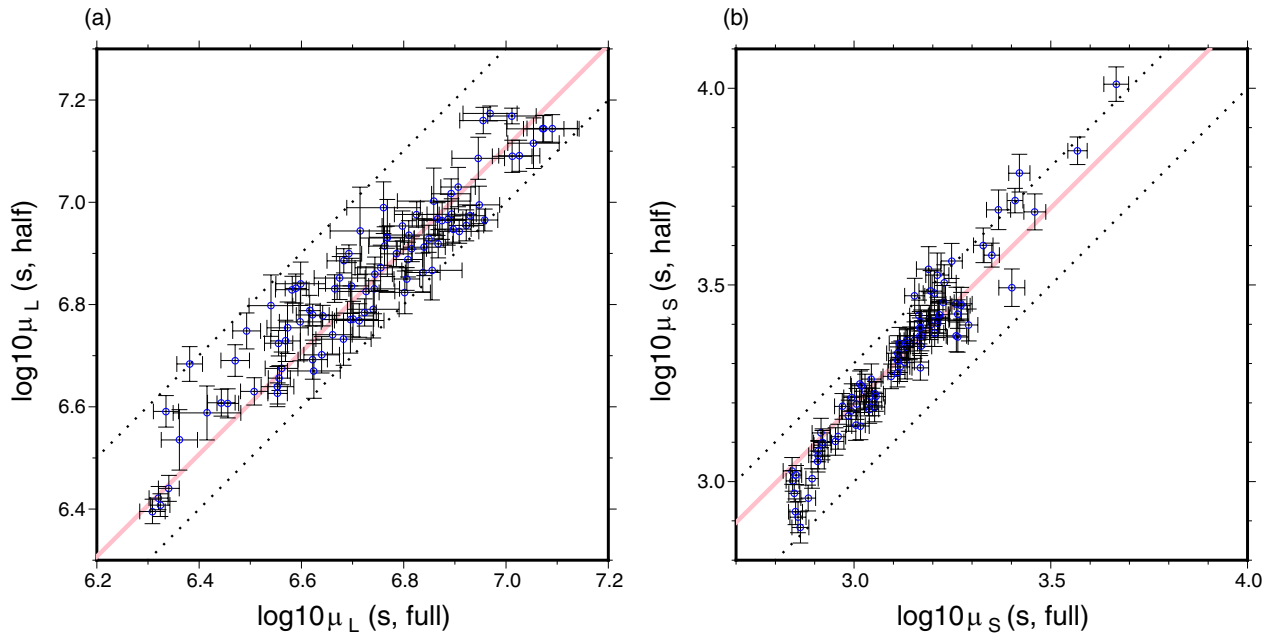

Fig. 10 Comparison of the parameter estimates obtained from the full catalog versus those obtained from one half of the catalog. **a** μ_L; **b** μ_S. Dashed lines denote the identity line (1:1 line; lower) and 1:2 line (upper), and red lines indicate the median of the estimated ratios

in one episodic activity. When μ_S is large, the change in μ_S is as large as that of a Poisson process, which suggests that the short-time recurrence is no longer periodic for these groups. We conclude from our test of an assumed very large change in tremor detectability (50%) that the present method reduces the effect of incomplete detectability to an extent because it evaluates the recurrence times, which are robust for small changes in detectability.

6.3 Extension to spatiotemporal models

This study used a time series of tremor activity that was spatially divided into groups at 0.05° intervals. However, this may not be appropriate because tremors interact with each other in both time and space. It is well known that tremors have a spatially segmented structure (Ide 2010; Obara 2010). While a small segment with tremors concentrated in a small area is safely assumed to be one group, large segments can extend over tens of kilometers, and tremor migration can occur over periods of a few days to weeks across multiple segments (e.g., Ito et al. 2007). Forecasting the activity of individual groups cannot be done independently, thereby requiring the degree of influence between groups to be quantified and incorporated into forecasting models for improved results.

Wang et al. (2018) proposed an approach to utilize the degree of this spatial influence by employing the hidden Markov model for the spatial clustering of tremors. They divided the tremors in each of the Kii and Shikoku regions into nearly 20 clusters, with the typical cluster size being larger than the size of the groups in this study and the clusters being divided into larger subsystems. Although there are few renewal process models that incorporate spatial effects, it is also possible to incorporate stress changes due to nearby events into the model as MRP, as was done to evaluate the tidal stress effects in the previous subsection. Alternatively, the external effects can be incorporated by transforming the time axis (Nomura and Tanaka 2021). These methods may provide more accurate forecasting capabilities if they incorporate the spatial effects of clustering and migration that were evaluated by Wang et al. (2018).

7 Conclusions

Scientific and social attention is often focused on whether slow deformation occurs near plate boundaries prior to a major earthquake, especially in the Nankai subduction zone, Japan. For monitoring this slow deformation at plate boundaries, tectonic tremors are a convenient phenomenon. Quantitative tremor monitoring is an important scientific and technical challenge, and it is also critical for improving our ability to make near-future predictions of tremor activity. However, few attempts have been made to forecast future tremor activity, due in part to the inability to accurately define individual events. Here, we set up a relatively simple forecasting problem in which the timing of the first tremor event after a given reference time is evaluated using the event time series

and a renewal process for each spatial group. The probability distribution of the renewal process was constructed as a mixture distribution of a BPT distribution, which represents long-term loading, and a log-normal distribution, which represents short-term interactions.

We estimated the parameters for this distribution following a well-established method for ordinary seismicity (e.g., Ogata 1988). We estimated five parameters that represented the mixture distribution via the maximum likelihood method using the EM algorithm and evaluated the goodness of fit of the model using the KS test. We were able to construct a model that explained the observed tremor intervals for 72% of all the analyzed groups. Some of the unsuccessful groups included temporary increases in the tremor occurrence rate due to a long-term SSE. However, we can objectively estimate the timing of occurrence of abnormal activity in these unsuccessful groups by dividing the groups into intervals using change points (Ogata 1992; Okutani and Ide 2011), which has also been used to determine earthquake swarms.

It is known that tremors with longer durations have longer recurrence periods (Idehara et al. 2014), but the converse is not true, as longer recurrence periods do not necessarily imply longer tremor durations. We employed two new parameters: the short-term recurrence period, which is expressed as a log-normal distribution, and the number of tremors during a single tremor episode, and found that the duration, short-term recurrence period, and number of tremors all affect the long-term recurrence interval. Furthermore, the rate of plate subduction is another important parameter, although previously estimated rates have large uncertainties. These dependencies are natural if we consider that episodic tremor activity releases the slip deficit accumulated by long-term loading during inter-episode periods.

We conducted a forecasting experiment using our renewal process model and the model parameters that were estimated from the previous 10-year period of tremor activity. We confirmed that the forecasting performance is almost as expected using the final 2.5-year period in the tremor catalog. Therefore, this model will be able to provide either daily or monthly tremor forecasts for the entire Nankai subduction zone. However, neither the 95% nor 68% prediction intervals can be very small, since the renewal process behavior is similar to a simple BPT model for long-term forecasting. Introducing spatial tremor interactions will be important for accurate forecasting, especially at short time scales.

Abbreviations

AIC: Akaike's information criterion; BPT: Brownian passage time; EM algorithm: Expectation–maximization algorithm; ETAS: Epidemic type aftershock sequence; KS test: Kolmogorov–Smirnov test; LFE: Low-frequency earthquake; MRP: Modulated renewal process; SSE: Slow-slip event; VLFE: Very-low-frequency earthquake.

Supplementary Information

The online version contains supplementary material available at https://doi.org/10.1186/s40645-022-00523-1.

Additional file 1: Figure S1. Histogram of interevent times shorter than 10,000 s for four groups: (a) 34.20°N, 134.05°E, (b) 34.65°N, 136.55°E, (c) 33.15°N, 132.25°E, and (d) 33.40°N, 132.80°E. The blue curve shows the estimated mixed model. The orange line shows the theoretical number of interevent times, produced from a Poisson process. **Figure S2**. Histogram of interevent time and estimated distribution for each group. In the histogram shown in blue, the fitted mixed distribution is overplotted with an orange curve. **Figure S3**. The estimated parameters for bootstrap samples for 4 groups shown in Fig. 2. (a) 34.20°N, 134.05°E, (b) 34.70°N, 136.55°E, (c) 33.15°N, 132.25°E, and (d) 33.40°N, 132.80°E. **Figure S4**. Spatial distribution of groups, for which the modeling was successful (white) or unsuccessful (red).

Additional file 2: Table S1. Estimated parameters in a CSV format file (ttf.csv).

Acknowledgements

We thank Takane Hori for providing the subduction velocity information for the Philippine Sea Plate. The comments from two anonymous reviewers and the editor Shoichi Yoshioka were all helpful to improve the manuscript.

Author contributions

SI proposed the strategy of the research, conducted data analysis, and prepared most of the text and figures/tables. SN developed statistical analysis tools. Both authors read and approved the final manuscript.

Funding

This research was supported by JSPS Kakenhi (21H04505), MEXT Kakenhi (21H05200), and the Earthquake and Volcano Hazards Observation and Research.

Availability of data and materials

The tectonic tremor catalog (Mizuno and Ide 2019) is provided by the slow earthquake database (Kano et al. 2018).

Declarations

Competing interests

The authors declare that they have no competing interests.

Author details

[1]Department of Earth and Planetary Science, The University of Tokyo, 7-3-1 Hongo, Bunkyo, Tokyo 113-0033, Japan. [2]Graduate School of Accountancy, Faculty of Commerce, Waseda University, 1-6-1 Nishiwaseda, Shinjuku, Tokyo 169-8050, Japan.

Received: 27 April 2022 Accepted: 17 November 2022
Published online: 08 December 2022

References

Aiken C, Obara K (2021) Data-driven clustering reveals more than 900 small magnitude slow earthquakes and their characteristics. Geophys Res Lett 48:e2020GL091764. https://doi.org/10.1029/2020GL091764

Ando M (1975) Source mechanisms and tectonic significance of historical earthquakes along the Nankai trough, Japan. Tectonophysics 27:119–140. https://doi.org/10.1016/0040-1951(75)90102-X

Ando R, Nakata R, Hori T (2010) A slip pulse model with fault heterogeneity for low-frequency earthquakes and tremor along plate interfaces. Geophys Res Lett 37:L10310. https://doi.org/10.1029/2010GL043056

Ando R, Takeda N, Yamashita T (2012) Propagation dynamics of seismic and aseismic slip governed by fault heterogeneity and Newtonian rheology. J Geophys Res Solid Earth 117:B11308. https://doi.org/10.1029/2012JB009532

Annoura S, Obara K, Maeda T (2016) Total energy of deep low-frequency tremor in the Nankai subduction zone, southwest Japan. Geophys Res Lett 43:2562–2567. https://doi.org/10.1002/2016GL067780
Bartlow NM, Miyazaki S, Bradley AM, Segall P (2011) Space-time correlation of slip and tremor during the 2009 Cascadia slow slip event. Geophys Res Lett. https://doi.org/10.1029/2011GL048714
Beeler NM, Thomas A, Bürgmann R, Shelly D (2013) Inferring fault rheology from low-frequency earthquakes on the San Andreas. J Geophys Res Solid Earth 118:5976–5990. https://doi.org/10.1002/2013JB010118
Beroza GC, Ide S (2011) Slow earthquakes and nonvolcanic tremor. Ann Rev Earth Planet Sci 39:271–296. https://doi.org/10.1146/annurev-earth-040809-152531
Brudzinski MR, Allen RM (2007) Segmentation in episodic tremor and slip all along Cascadia. Geology 35:907–910. https://doi.org/10.1130/G23740A.1
Cox DR (1972) The statistical analysis of dependencies in point processes. In: Lewis PAW (ed) Stochastic point processes. Wiley, New York, pp 55–66
Dempster AP, Laird NM, Rubin DB (1977) Maximum likelihood from incomplete data via the EM algorithm. J R Stat Soc Ser B 39:1–38
Dragert H, Wang K, Rogers G (2004) Geodetic and seismic signatures of episodic tremor and slip in the northern Cascadia subduction zone. Earth Planets Space 56:1143–1150. https://doi.org/10.1186/BF03353333
Dziewonski AM, Anderson DL (1981) Preliminary reference earth model. Phys Earth Planet Int 25:297–356. https://doi.org/10.1016/0031-9201(81)90046-7
Efron B, Tibshirani RJ (1993) An introduction to the Bootstrap. Springer, New York. https://doi.org/10.1007/978-1-4899-4541-9
Farge G, Jaupart C, Shapiro NM (2021) Episodicity and migration of low frequency earthquakes modeled with fast fluid pressure transients in the permeable subduction interface. J Geophys Res Solid Earth 126:e2021JB021894. https://doi.org/10.1029/2021JB021894
Frank WB, Shapiro NM, Husker AL, Kostoglodov V, Gusev AA, Campillo M (2016) The evolving interaction of low-frequency earthquakes during transient slip. Sci Adv. https://doi.org/10.1126/sciadv.1501616
Ghosh A, Vidale JE, Sweet JR, Creager KC, Wech AG, Houston H, Brodsky EE (2010) Rapid, continuous streaking of tremor in Cascadia. Geochem Geophys Geosyst. https://doi.org/10.1029/2010GC003305
Hashimoto M (2022) Is the long-term probability of the occurrence of large earthquakes along the Nankai Trough inflated? Scientific review. Seismol Res Lett 93:2311–2319. https://doi.org/10.1785/0220210152
Heki K, Miyazaki S (2001) Plate convergence and long-term crustal deformation in central Japan. Geophys Res Lett 28:2313–2316. https://doi.org/10.1029/2000GL012537
Hirose H, Obara K (2010) Recurrence behavior of short-term slow slip and correlated nonvolcanic tremor episodes in western Shikoku, southwest Japan. J Geophys Res. https://doi.org/10.1029/2008JB006050
Hori T, Kato N, Hirahara K, Baba T, Kaneda Y (2004) A numerical simulation of earthquake cycles along the Nankai Trough in southwest Japan: lateral variation in frictional property due to the slab geometry controls the nucleation position. Earth Planet Sci Lett 228:215–226. https://doi.org/10.1016/j.epsl.2004.09.033
Houston H, Delbridge BG, Wech AG, Creager KC (2011) Rapid tremor reversals in Cascadia generated by a weakened plate interface. Nat Geosci 4:404–409. https://doi.org/10.1038/ngeo1157
Ide S (2010) Striations, duration, migration and tidal response in deep tremor. Nature 466:356–359. https://doi.org/10.1038/nature09251
Ide S (2012) Variety and spatial heterogeneity of tectonic tremor worldwide. J Geophys Res Solid Earth. https://doi.org/10.1029/2011JB008840
Ide S (2019) Detection of low-frequency earthquakes in broadband random time sequences: are they independent events? J Geophys Res Solid Earth 124:8611–8625. https://doi.org/10.1029/2019JB017643
Ide S, Tanaka Y (2014) Controls on plate motion by oscillating tidal stress: Evidence from deep tremors in western Japan. Geophys Res Lett 41:3842–3850. https://doi.org/10.1002/2014GL060035
Ide S, Yabe S (2014) Universality of slow earthquakes in the very low frequency band. Geophys Res Lett 41:2786–2793. https://doi.org/10.1002/2014GL059712
Ide S, Beroza GC, Shelly DR, Uchide T (2007) A scaling law for slow earthquakes. Nature 447:76–79. https://doi.org/10.1038/nature05780
Idehara K, Yabe S, Ide S (2014) Regional and global variations in the temporal clustering of tectonic tremor activity. Earth Planets Space 66:66. https://doi.org/10.1186/1880-5981-66-66
Ito Y, Obara K, Shiomi K, Sekine S, Hirose H (2007) Slow earthquakes coincident with episodic tremors and slow slip events. Science 315:503–506. https://doi.org/10.1126/science.1134454
Ito Y, Hino R, Kido M, Fujimoto H, Osada Y, Inazu D, Ohta Y, Iinuma T, Ohzono M, Miura S, Mishina M, Suzuki K, Tsuji T, Ashi J (2013) Episodic slow slip events in the Japan subduction zone before the 2011 Tohoku-Oki earthquake. Tectonophysics 600:14–26. https://doi.org/10.1016/j.tecto.2012.08.022
Jordan TH (2006) Earthquake predictability, brick by brick. Seismol Res Lett 77:3–6. https://doi.org/10.1785/gssrl.77.1.3
Kano M, Aso N, Matsuzawa T, Ide S, Annoura S, Arai R, Baba S, Bostock M, Chao K, Heki K, Itaba S, Ito Y, Kamaya N, Maeda T, Maury J, Nakamura M, Nishimura T, Obana K, Ohta K, Poiata N, Rousset B, Sugioka H, Takagi R, Takahashi T, Takeo A, Tu Y, Uchida N, Yamashita Y, Obara K (2018) Development of a slow earthquake database. Seismol Res Lett 89:1566–1575. https://doi.org/10.1785/0220180021
Kobayashi A (2017) Objective detection of long-term slow slip events along the Nankai Trough using GNSS data (1996–2016). Earth Planets Space 69:171. https://doi.org/10.1186/s40623-017-0755-7
Kostoglodov V, Husker A, Shapiro NM, Payero JS, Campillo M, Cotte N, Clayton R (2010) The 2006 slow slip event and nonvolcanic tremor in the Mexican subduction zone. Geophys Res Lett. https://doi.org/10.1029/2010GL045424
Kumazawa T, Ogata Y, Kimura K, Maeda K, Kobayashi A (2016) Background rates of swarm earthquakes that are synchronized with volumetric strain changes. Earth Planet Sci Lett 442:51–60. https://doi.org/10.1016/j.epsl.2016.02.049
Llenos AL, McGuire JJ, Ogata Y (2009) Modeling seismic swarms triggered by aseismic transients. Earth Planet Sci Lett 281:59–69. https://doi.org/10.1016/j.epsl.2009.02.011
Masuda K, Ide S, Ohta K, Matsuzawa T (2020) Bridging the gap between low-frequency and very-low-frequency earthquakes. Earth Planets Space 72:47. https://doi.org/10.1186/s40623-020-01172-8
Matsuzawa T, Hirose H, Shibazaki B, Obara K (2010) Modeling short- and long-term slow slip events in the seismic cycles of large subduction earthquakes. J Geophys Res Solid Earth. https://doi.org/10.1029/2010JB007566
Matthews MV, Ellsworth WL, Reasenberg PA (2002) A Brownian model for recurrent earthquakes. Bull Seismol Soc Am 92:2233–2250. https://doi.org/10.1785/0120010267
Miyazaki S, Heki K (2001) Crustal velocity field of southwest Japan: subduction and arc-arc collision. J Geophys Res Solid Earth 106:4305–4326. https://doi.org/10.1029/2000JB900312
Miyazaki S, Segall P, McGuire JJ, Kato T, Hatanaka Y (2006) Spatial and temporal evolution of stress and slip rate during the 2000 Tokai slow earthquake. J Geophys Res Solid Earth. https://doi.org/10.1029/2004JB003426
Miyazawa M, Brodsky EE (2008) Deep low-frequency tremor that correlates with passing surface waves. J Geophys Res Solid Earth. https://doi.org/10.1029/2006JB004890
Mizuno N, Ide S (2019) Development of a modified envelope correlation method based on maximum-likelihood method and application to detecting and locating deep tectonic tremors in western Japan. Earth Planets Space 71:40. https://doi.org/10.1186/s40623-019-1022-x
Nakata R, Suda N, Tsuruoka H (2008) Non-volcanic tremor resulting from the combined effect of Earth tides and slow slip events. Nat Geosci 1:676–678. https://doi.org/10.1038/ngeo288
Nakata R, Ando R, Hori T, Ide S (2011) Generation mechanism of slow earthquakes: numerical analysis based on a dynamic model with brittle-ductile mixed fault heterogeneity. J Geophys Res Solid Earth. https://doi.org/10.1029/2010JB008188
Nomura S, Tanaka M (2021) Forecasting repeating earthquakes considering aftershock triggering effects (in Japanese). Proc Inst Stat Math 69:239–254
Obara K (2002) Nonvolcanic deep tremor associated with subduction in southwest Japan. Science 296:1679–1681. https://doi.org/10.1126/science.1070378
Obara K (2010) Phenomenology of deep slow earthquake family in southwest Japan: spatiotemporal characteristics and segmentation. J Geophys Res Solid Earth. https://doi.org/10.1029/2008JB006048
Obara K, Kato A (2016) Connecting slow earthquakes to huge earthquakes. Science 353:253–257. https://doi.org/10.1126/science.aaf1512

Ogata Y (1988) Statistical models for earthquake occurrences and residual analysis for point processes. J Am Stat Assoc 83:9–27. https://doi.org/10.1080/01621459.1988.10478560
Ogata Y (1992) Detection of precursory relative quiescence before great earthquakes through a statistical model. J Geophys Res Solid Earth 97:19845–19871. https://doi.org/10.1029/92JB00708
Ogata Y (2005) Detection of anomalous seismicity as a stress change sensor. J Geophys Res Solid Earth. https://doi.org/10.1029/2004JB003245
Okutani T, Ide S (2011) Statistic analysis of swarm activities around the Boso Peninsula, Japan: slow slip events beneath Tokyo Bay? Earth Planets Space 63:419–426. https://doi.org/10.5047/eps.2011.02.010
Rubinstein JL, La Rocca M, Vidale JE, Creager KC, Wech AG (2008) Tidal modulation of nonvolcanic tremor. Science 319:186–189. https://doi.org/10.1126/science.1150558
Shelly DR (2010) Migrating tremors illuminate complex deformation beneath the seismogenic San Andreas fault. Nature 463:648–652. https://doi.org/10.1038/nature08755
Shelly DR, Johnson KM (2011) Tremor reveals stress shadowing, deep postseismic creep, and depth-dependent slip recurrence on the lower-crustal San Andreas fault near Parkfield. Geophys Res Lett. https://doi.org/10.1029/2011GL047863
Shelly DR, Beroza GC, Ide S (2007a) Non-volcanic tremor and low-frequency earthquake swarms. Nature 446:305–307. https://doi.org/10.1038/nature05666
Shelly DR, Beroza GC, Ide S (2007) Complex evolution of transient slip derived from precise tremor locations in western Shikoku, Japan. Geochem Geophys Geosyst. https://doi.org/10.1029/2007GC001640
Thomas AM, Bürgmann R, Shelly DR, Beeler NM, Rudolph ML (2012) Tidal triggering of low frequency earthquakes near Parkfield, California: implications for fault mechanics within the brittle-ductile transition. J Geophys Res Solid Earth. https://doi.org/10.1029/2011JB009036
van der Elst NJ, Delorey AA, Shelly DR, Johnson PA (2016) Fortnightly modulation of San Andreas tremor and low-frequency earthquakes. PNAS 113:8601–8605. https://doi.org/10.1073/pnas.1524316113
Wang T, Zhuang J, Buckby J, Obara K, Tsuruoka H (2018) Identifying the recurrence patterns of nonvolcanic tremors using a 2-D hidden Markov model with extra zeros. J Geophys Res Solid Earth 123:6802–6825. https://doi.org/10.1029/2017JB015360
Wech AG, Creager KC (2008) Automated detection and location of Cascadia tremor. Geophys Res Lett. https://doi.org/10.1029/2008GL035458
Wech AG, Creager KC (2011) A continuum of stress, strength and slip in the Cascadia subduction zone. Nature Geosci 4:624–628. https://doi.org/10.1038/ngeo1215
Yabe S, Tanaka Y, Houston H, Ide S (2015) Tidal sensitivity of tectonic tremors in Nankai and Cascadia subduction zones. J Geophys Res Solid Earth 120:7587–7605. https://doi.org/10.1002/2015JB012250
Yoshioka S, Matsuoka Y, Ide S (2015) Spatiotemporal slip distributions of three long-term slow slip events beneath the Bungo Channel, southwest Japan, inferred from inversion analyses of GPS data. Geophys J Int 201:1437–1455. https://doi.org/10.1093/gji/ggv022

Publisher's Note

Springer Nature remains neutral with regard to jurisdictional claims in published maps and institutional affiliations.

Submit your manuscript to a SpringerOpen journal and benefit from:

- ► Convenient online submission
- ► Rigorous peer review
- ► Open access: articles freely available online
- ► High visibility within the field
- ► Retaining the copyright to your article

Submit your next manuscript at ► springeropen.com